

Article

The Spatio-Temporal Dynamics of Water Resources (Rainfall and Snow) in the Sierra Nevada Mountain Range (Southern Spain)

Eulogio Pardo-Igúzquiza ^{1,*}, Sergio Martos-Rosillo ², Jorge Jódar ³ and Peter A. Dowd ⁴¹ Instituto de Geociencias (CSIC-UCM), Severo Ochoa, Planta 4, 28040 Madrid, Spain² Instituto Geológico y Minero de España (IGME, CSIC), Unidad de Granada, Urbanización Alcázar del Genil, 4. Edificio Zulema, 18006 Granada, Spain; s.martos@igme.es³ IGME, CSIC, Unidad de Zaragoza, Manuel Lasala 44, 9B, 50006 Zaragoza, Spain; j.jodar@igme.es⁴ Faculty of Sciences, Engineering and Technology, The University of Adelaide, Adelaide 5005, Australia; peter.dowd@adelaide.edu.au

* Correspondence: e.pardo.iguzquiza@csic.es

Abstract: This paper describes the use of a unique spatio-temporally resolved precipitation and temperature dataset to assess the spatio-temporal dynamics of water resources over a period of almost seven decades across the Sierra Nevada mountain range, which is the most southern Alpine environment in Europe. The altitude and geographical location of this isolated alpine environment makes it a good detector of climate change. The data were generated by applying geostatistical co-kriging to significant instrumental precipitation and temperature (minimum, maximum and mean) datasets. The correlation between precipitation and altitude was not particularly high and the statistical analysis yielded some surprising results in the form of mean annual precipitation maps and yearly precipitation time series. These results confirm the importance of orographic precipitation in the Sierra Nevada mountain range and show a decrease in mean annual precipitation of 33 mm per decade. Seasonality, however, has remained constant throughout the period of the study. The results show that previous studies have overestimated the altitudinal precipitation gradient in the Sierra Nevada and reveal its complex spatial variability. In addition, the results show a clear correspondence between the mean annual precipitation and the NAO index and, to a much lesser extent, the WeMO index. With respect to temperature, there is a high correlation between minimum temperature and altitude (coefficient of correlation = -0.84) and between maximum temperature and altitude (coefficient of correlation = -0.9). Thus, our spatial temperature maps were very similar to topographic maps, but the temporal trend was complex, with negative (decreasing) and positive (increasing) trends. A dynamic model of snowfall can be obtained by using the degree-day methodology. These results should be considered when checking the local performance of climatological models.

Keywords: high mountain climatology; orographic rainfall; alpine environment; temperatures; snow; NAO index; WeMO index; rain gauges; co-kriging



Citation: Pardo-Igúzquiza, E.; Martos-Rosillo, S.; Jódar, J.; Dowd, P.A. The Spatio-Temporal Dynamics of Water Resources (Rainfall and Snow) in the Sierra Nevada Mountain Range (Southern Spain). *Resources* **2024**, *13*, 42. <https://doi.org/10.3390/resources13030042>

Academic Editor: Antonio A. R. Ioris

Received: 9 January 2024

Revised: 27 February 2024

Accepted: 28 February 2024

Published: 12 March 2024



Copyright: © 2024 by the authors. Licensee MDPI, Basel, Switzerland. This article is an open access article distributed under the terms and conditions of the Creative Commons Attribution (CC BY) license (<https://creativecommons.org/licenses/by/4.0/>).

1. Introduction

Mountains play an important role in the Earth System and the availability of water resources. They cover 25% of the global land surface, provide living space for 26% of the world's population [1,2], supply freshwater resources to surrounding lowlands, and host a significant amount of biodiversity. Mountain environments are highly sensitive to changes in climate [3] and are sensors for early detection of climate change [4]. The high sensitivity of mountain environments to climate change has generated significant research to improve climate observations at high elevations [5]. The alpine regions of the Mediterranean are among the most climatically sensitive areas in the world [6]. In many areas of the world, climate monitoring in high altitude regions continues to be sparse and of low quality; observation networks are deficient and climate values are estimated by extrapolating from

low-altitude data. This can be particularly misleading when extrapolating precipitation. There appears to be a general positive correlation between precipitation and altitude [7,8], but it is not as simple and direct as the high (negative) correlation between temperature and altitude [9,10].

The focus of the work presented here is a study on the spatio-temporal dynamics of precipitation and temperature in the high-altitude Sierra Nevada mountain range in Southern Spain in order to evaluate the spatio-temporal dynamics of water resources in the form of rainfall and snow. There have been many studies on precipitation in Southern Spain. For example, various aspects of precipitation in the Mediterranean region of Spain are considered in [11,12]. The authors of [13] studied daily precipitation in Spain for the period of 1951 to 2002 using data from 22 sites. The authors of [14] studied seasonal trends in precipitation in the Mediterranean Iberian peninsula from 1951 to 2000. The authors of [15] studied dry periods over the pluviometric gradient (from Gibraltar to Almeria) in Mediterranean southern Spain. The authors of [16] provided a database of gridded precipitation and temperature in Spain for the 1950–2003 period, but the grid spacing they used had a horizontal resolution of approximately 20 km.

These and other previous studies have estimated precipitation and temperature over large regions, such as the entire Mediterranean region or the whole of the Iberian Peninsula, without any altitudinal restriction. The work presented here focuses on precipitation and temperature within the high-altitude area of the Sierra Nevada mountain range, and specifically, on the connected region with altitudes from 1500 m above sea level (asl) to almost 3500 m asl, which comprises the most southern alpine environment in Europe. The objective was to build a database of daily precipitation and temperature within this high-altitude area and to interpret it by using various statistical analyses, as explained in the following sections. This database reveals the spatio-temporal evolution of water resources in the studied area.

2. Methodology

Estimating precipitation in mountainous areas is a problem of recent interest [17,18]. There are particular solutions to the general problem of evaluating the areal distribution of precipitation using limited precipitation records (see for example [19,20] for urban areas). However, geostatistics has proved to be the optimal technique for estimating daily precipitation and daily temperature using altitude as a secondary variable [21–23], among others. Altitude data are readily available from digital elevation models (DEMs) which provide complete coverage of an area. Rainfall data, however, are limited to sparsely located rain gauges. Temperature data are even more sparse, although they show a higher (negative) correlation with altitude. There are various geostatistical kriging procedures for incorporating altitude as a secondary variable. The most widely used is co-kriging [24], which is a multivariate geostatistical interpolator [25]. Essentially, the relative scarcity of the directly measured data for the primary variable (precipitation or temperature) is compensated for by using its spatial correlation with the more abundant secondary variable (altitude). The application of co-kriging requires estimates of the direct variogram (or covariance) of precipitation (or temperature), the direct variogram (or covariance) of altitude, and the cross-variogram (or cross-covariance) of precipitation and altitude (or temperature and altitude). These three estimated variograms are modelled by fitting permissible models, of which the most widely used is the linear co-regionalisation model [26]. Co-kriging is used to estimate daily precipitation and temperature on a regular grid, and seasonal and annual averages are estimated by summing the days contained in the chosen time period (or support in geostatistical terminology) of estimation (e.g., one month, one season, one year). As the number of rain gauges and temperature stations available for any particular day may be small, a climatological variogram is used [27,28]. The shape and range of the climatological variogram remains constant, while the nugget variance and partial sill are updated with daily precipitation and temperature statistics [28]. The mathematical basics of co-kriging are considered next.

Co-kriging is a geostatistical method for optimal multivariate spatial interpolation [26]. In geostatistics, spatial variable $Z(\mathbf{u})$ at spatial location \mathbf{u} , representing, for example rainfall, minimum temperature, maximum temperature, etc., is modelled as a random variable. The set of all random variables $Z(\mathbf{u})$ in region χ of the space, $\mathbf{u} \in \chi$, comprises a random function or random field $Z(\mathbf{u})$. With $\chi \subset \mathbb{R}^d$ and $d = 2$, the problem is two-dimensional, as is the case in the work presented here for precipitation or temperature and elevation. Thus, $Z(\mathbf{u})$ represents precipitation or temperature and is the variable of interest that is to be estimated by co-kriging.

It is assumed that $Z(\mathbf{u})$ is second-order stationary with constant spatial mean

$$E\{Z(\mathbf{u})\} = m_Z, \quad (1)$$

and the two-point statistics, the covariance, and the variogram functions depend only on vector \mathbf{h} :

$$C_Z(\mathbf{u}, \mathbf{u} + \mathbf{h}) = C_Z(\mathbf{h}) = E\{Z(\mathbf{u})Z(\mathbf{u} + \mathbf{h})\} - m_Z^2, \quad (2)$$

$$\gamma_Z(\mathbf{h}) = C_Z(0) - C_Z(\mathbf{h}), \quad (3)$$

$$C_Z(0) = \sigma_Z^2. \quad (4)$$

where m_Z , σ_Z^2 , $\gamma_Z(\mathbf{h})$ and $C_Z(\mathbf{h})$ are, respectively, the mean, variance, variogram, and covariance of the random function $Z(\mathbf{u})$ and $E\{\cdot\}$ is the mathematical expectation operator.

In the simplest form of co-kriging, a variable of interest, or primary variable (e.g., temperature or precipitation), is estimated based on the experimental values of the variable and the experimental values of a secondary variable (e.g., altitude) that is correlated with the primary variable. The co-kriging estimator of the precipitation (or temperature) at any given geographical location $\mathbf{u}_0 = \{x_0, y_0\}$, where $\{x_0, y_0\}$ are the easting and northing coordinates respectively, can be expressed as:

$$Z \times (\mathbf{u}_0) = \sum_{i=1}^n \lambda_i^0 Z(\mathbf{u}_i) + \sum_{j=1}^m \beta_j^0 Y(\mathbf{u}_j). \quad (5)$$

where:

$Z(\mathbf{u})$ is the primary variable, precipitation or temperature, at location \mathbf{u} , and $Y(\mathbf{u})$ is the secondary variable, altitude, at location \mathbf{u} .

n and m are the number of values of variables $Z(\mathbf{u})$ and $Y(\mathbf{u})$, respectively, used in the estimation in Equation (5). Usually, these data are inside a neighbourhood centred on estimation location \mathbf{u}_0 .

The optimal weights for the linear estimation in Equation (5) are obtained by solving the corresponding co-kriging system; see for example, refs. [25,29]. If only the primary variable is used, ordinary co-kriging reduces to ordinary kriging of the primary variable. The same applies if there is no correlation between the primary and secondary variables.

For co-kriging, the direct variograms of the two variables and the cross-variogram (or direct covariances and cross-covariance) between the two variables must be estimated from the experimental data.

The unbiasedness of the co-kriging estimator in Equation (5) implies that the mean estimation error is zero:

$$E\{Z \times (\mathbf{u}_0) - Z(\mathbf{u}_0)\} = 0. \quad (6)$$

This is achieved by including the following conditions in the co-kriging system:

$$\sum_{i=1}^n \lambda_i^0 = 1, \quad (7)$$

and

$$\sum_{k=1}^m \beta_k^0 = 0, \tag{8}$$

The variance of the estimation error can be written as:

$$\begin{aligned} \text{Var}\{Z \times (\mathbf{u}_0) - Z(\mathbf{u}_0)\} &= \sum_{i=1}^n \sum_{j=1}^n \lambda_i^0 \lambda_j^0 C_Z(\mathbf{h}_{ij}) + \sum_{i=1}^m \sum_{j=1}^m \beta_i^0 \beta_j^0 C_Y(\mathbf{h}_{ij}) \\ &+ \sum_{i=1}^n \sum_{j=1}^m \lambda_i^0 \beta_j^0 C_{ZY}(\mathbf{h}_{ij}) + \sum_{j=1}^m \sum_{i=1}^n \beta_j^0 \lambda_i^0 C_{YZ}(\mathbf{h}_{ji}) \\ &- 2 \sum_{i=1}^n \lambda_i^0 C_Z(\mathbf{h}_{i0}) - 2 \sum_{j=1}^m \beta_j^0 C_Y(\mathbf{h}_{j0}) + C_Z(\mathbf{h}_{00}), \end{aligned} \tag{9}$$

The co-kriging system is obtained by minimising the estimated variance in Equation (1), subject to the unbiasedness conditions, which, in matrix form [30], is:

$$\mathbf{C}\boldsymbol{\lambda} = \mathbf{B}, \tag{10}$$

with:

$$\mathbf{C} = \begin{bmatrix} C_Z(\mathbf{h}_{11}) & \cdots & C_Z(\mathbf{h}_{1n}) & C_{ZY}(\mathbf{h}_{11}) & \cdots & C_{ZY}(\mathbf{h}_{1m}) & 1 & 0 \\ \vdots & \ddots & \vdots & \vdots & \ddots & \vdots & \vdots & \vdots \\ C_Z(\mathbf{h}_{n1}) & \cdots & C_Z(\mathbf{h}_{nn}) & C_{ZY}(\mathbf{h}_{n1}) & \cdots & C_{ZY}(\mathbf{h}_{nm}) & 1 & 0 \\ C_{YZ}(\mathbf{h}_{11}) & \cdots & C_{YZ}(\mathbf{h}_{1n}) & C_Y(\mathbf{h}_{11}) & \cdots & C_Y(\mathbf{h}_{1m}) & 0 & 1 \\ \vdots & \ddots & \vdots & \vdots & \ddots & \vdots & \vdots & \vdots \\ C_{YZ}(\mathbf{h}_{m1}) & \cdots & C_{YZ}(\mathbf{h}_{mn}) & C_Y(\mathbf{h}_{m1}) & \cdots & C_Y(\mathbf{h}_{mm}) & 0 & 1 \\ 1 & \cdots & 1 & 0 & \cdots & 0 & 0 & 0 \\ 0 & \cdots & 0 & 1 & \cdots & 1 & 0 & 0 \end{bmatrix} \tag{11}$$

$$\boldsymbol{\lambda} = \begin{bmatrix} \lambda_1^0 \\ \vdots \\ \lambda_n^0 \\ \beta_1^0 \\ \vdots \\ \beta_m^0 \\ \mu_1 \\ \mu_2 \end{bmatrix}, \mathbf{B} = \begin{bmatrix} C_Z(\mathbf{h}_{10}) \\ \vdots \\ C_Z(\mathbf{h}_{n0}) \\ C_{ZY}(\mathbf{h}_{01}) \\ \vdots \\ C_{ZY}(\mathbf{h}_{0m}) \\ 1 \\ 0 \end{bmatrix} \tag{12}$$

where μ_1 and μ_2 are Lagrange multipliers or parameters that are used to include the constraints given in Equations (7) and (8).

The solution of the co-kriging system:

$$\boldsymbol{\lambda} = \mathbf{C}^{-1}\mathbf{B}, \tag{13}$$

provides the weights required in the estimator in Equation (5).

In the geostatistical literature, the form of co-kriging summarised above is known as “ordinary co-kriging” to distinguish it from “simple co-kriging”, in which the mean m_Z in Equation (1) is known [26,29,31].

3. Case Study

The isolated Sierra Nevada mountain range (Figure 1), in the Andalucía region of southern Spain, has an E–W orientation and dimensions of around 70 km in the E–W direction and a mean of 20 km in the N–S direction, although its width decreases from West to East. The total area of the mountain range is around 1360 km². The Mulhacen Peak, at 3479 m asl, is the highest altitude in the Iberian Peninsula and is located at longitude 3.312°

W and latitude 37.053° N. This mountain range is at an ideal location to monitor climate change because it is an isolated alpine environment at, for Europe, a relatively low latitude.

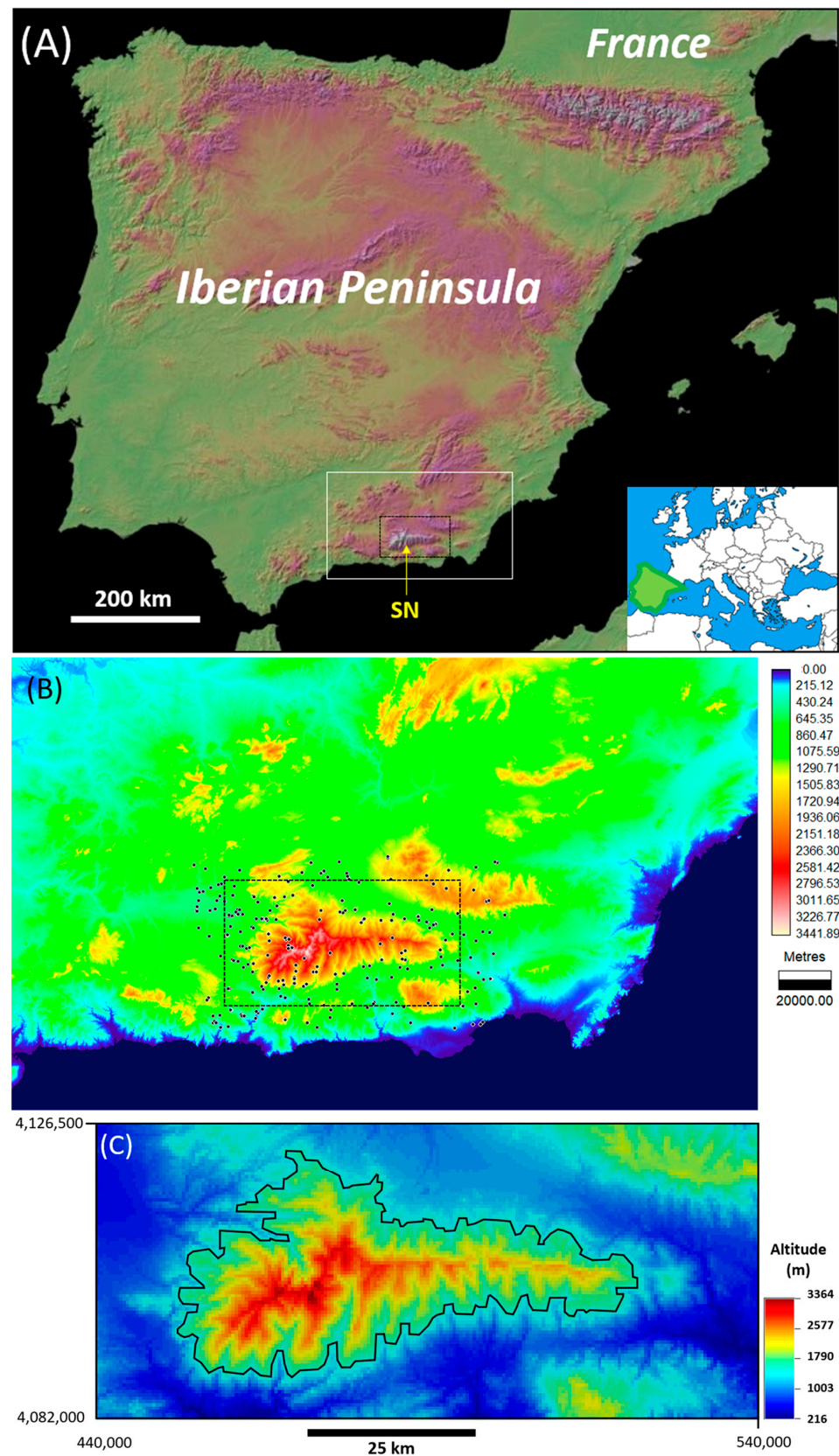


Figure 1. Geographical location of the study area, the Sierra Nevada (SN) mountain range in southern Spain. (A). General location of SN in southern Spain. The white rectangle represents the area shown

in (B) and the black rectangle represents the area shown in (C). (B). Digital elevation model of the regional context of the Sierra Nevada mountain range in the middle of the image enclosed by the dashed black rectangle. The colour scale represents altitude in metres above sea level. The black dots represent the locations of rain gauges where the experimental data were measured. (C). Digital elevation model with the colour scale representing altitude above sea level in metres. This area represents the estimation grid comprising 201 columns and 90 rows with a spacing of 500 m in the E–W direction and 500 m in the N–S direction. A black polygon encloses the connected area that has an altitude higher than 1500 m. This polygon is the high-altitude area of Sierra Nevada from which areal or integrated values were obtained from the grid estimates. The geographical coordinates in Figure 1C are in the Universal Transverse Mercator (UTM) projection.

Almost seven decades (67 years from 1951 to 2017) of precipitation and temperature data, measured at 247 stations (rain gauges and temperature stations), are shown in Figure 1B. Not all the stations were in operation for the entire period, and the network has changed over time. For example, Figure 2 shows the evolution over time of the mean number of operating precipitation (rain gauges) and temperature stations. The number of operating rain gauges increased steadily during the 1950s and 1960s and reached a mean number of around 70 rain gauges during the 1970s and 1980s, increasing thereafter to a mean of 90 rain gauges from the 1990s until the last year of the study, i.e., 2017. Over the last 20 years of this sequence, there was a high degree of variability in the number of operating rain gauges, but the total number was never less than 50. The number of operating temperature stations has also increased steadily since 1951, but usually their number is around a third of the number of rain gauges.

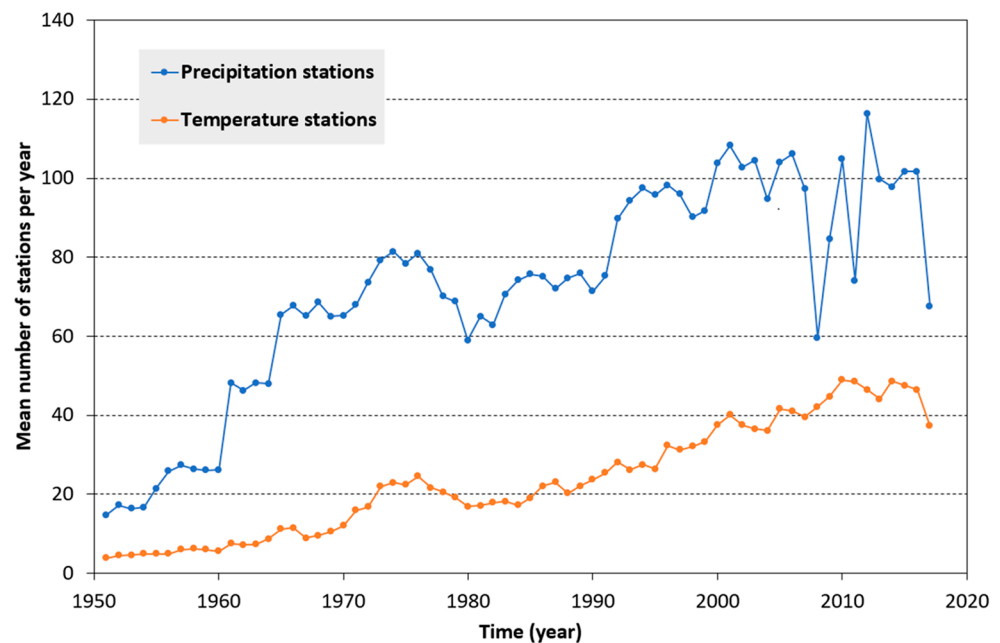


Figure 2. Mean annual number of precipitation and temperature monitoring stations from 1951 to 2017. The locations of the precipitation stations are shown in Figure 1B as solid black dots.

Daily precipitation and temperature were estimated for the 67 years of the study, which involved the spatial estimation of these variables for 24,471 days. The estimation network has a spacing of 500 m in each of the X and Y directions. The estimation network has 201 columns and 90 rows (Figure 1C) but the statistics were calculated for the area of the Sierra Nevada mountain range, restricted to the black polygon in Figure 1C and representing a connected area with altitudes higher than 1500 m. This altitude of 1500 m was selected on the basis that it delineates very well the isolated alpine massif of Sierra Nevada, as can be seen in Figure 1C.

4. Results

Geostatistical co-kriging was applied to the database of experimental precipitation and temperature data. The linear regionalisation model was used with a spherical variogram model with a range of 30 km and a nugget variance and partial sill that were updated each day according to the daily variance of precipitation and temperature, i.e., following the methodology of the climatological variogram. The result is a new database comprising daily precipitation and temperature (minimum, maximum and mean) for 67 years on a 500 m × 500 m spatial grid (Figure 1C).

Using the new database, various averages in space and time can be calculated to highlight the spatio-temporal dynamics of precipitation and temperature for the Sierra Nevada mountain range. As shown in Figure 1C, the mountain range has been defined by including all points of the estimation grid that have an altitude greater than 1500 m and that yield a connected polygon that clearly defines the Sierra Nevada mountain range.

The first important result is the mean annual precipitation in the Sierra Nevada for the period from 1951 to 2017, which is represented in Figure 3. Figure 3A shows a raster colour map and Figure 3B shows lines of equal precipitation (isohyets) overlaying the raster DEM in Figure 1C. The most surprising result is the strong orographic influence in the spatial distribution of the mean annual precipitation. The most striking fact is that the dome of maximum precipitation has an NW–SE orientation rather than the E–W main topographical orientation of the Sierra Nevada orographic dome, as reported in most previous studies. The second interesting result is that the maximum coincides with the summit of the range but is in the upper part of the main valley of the southern slope. The third surprising result is that there is a second relative maximum (2 in Figure 3A) in the eastern part of the Sierra, also located on the southern slope. There is also a second maximum of annual rainfall (3 in Figure 3A), but it is located outside, and northwest of, the Sierra Nevada mountain range.

The estimated map of mean annual precipitation (Figure 3A) is consistent with Figure 2 of Sumner et al. (2003) [32], which represents the average annual precipitation (mm) for 1964–1993, but not with the detail given in the work presented here. In addition, the Confederación Hidrográfica del Guadalquivir (Water authority for the management of the Guadalquivir river basin) reported a mean precipitation of 618 mm in the river basin of the Canales dam (with a surface of 176 km²). A similar estimate of 633 mm was obtained for the areal value for the same river basin in the map in Figure 3A.

Another interesting result is the map of mean precipitation for the 1951–2017 period, but instead of integrating time for the year, it is integrated for each season: Spring (April, May, June), Summer (July, August, September), Autumn (October, November, December), and Winter (January, February, March). The results are shown in Figure 4 and can be interpreted as a decomposition of the mean annual precipitation in Figure 3 to produce the mean precipitation by season. This map should be assessed in conjunction with the results shown in Table 1, which shows the mean precipitation by month and season. Table 1 shows that, climatologically, the driest month is July, with less than 1% of the annual precipitation, while the wettest month is December, with 15% of the yearly precipitation. August is also a dry month, with 1.2% of the annual precipitation, while June and September, with 3.1% and 4.9% respectively of the annual precipitation, can be considered intermediate months. The remaining months, from October to May, can be considered humid months that define the rainy season. The seasons, from wettest to driest, are Autumn, Winter, Spring and Summer, with 39%, 34%, 20% and 7% respectively of the annual precipitation. The mean annual precipitation for Sierra Nevada for the 1951–2017 period is 575 mm with a standard deviation of 191 mm; this implies a high variability from year to year.

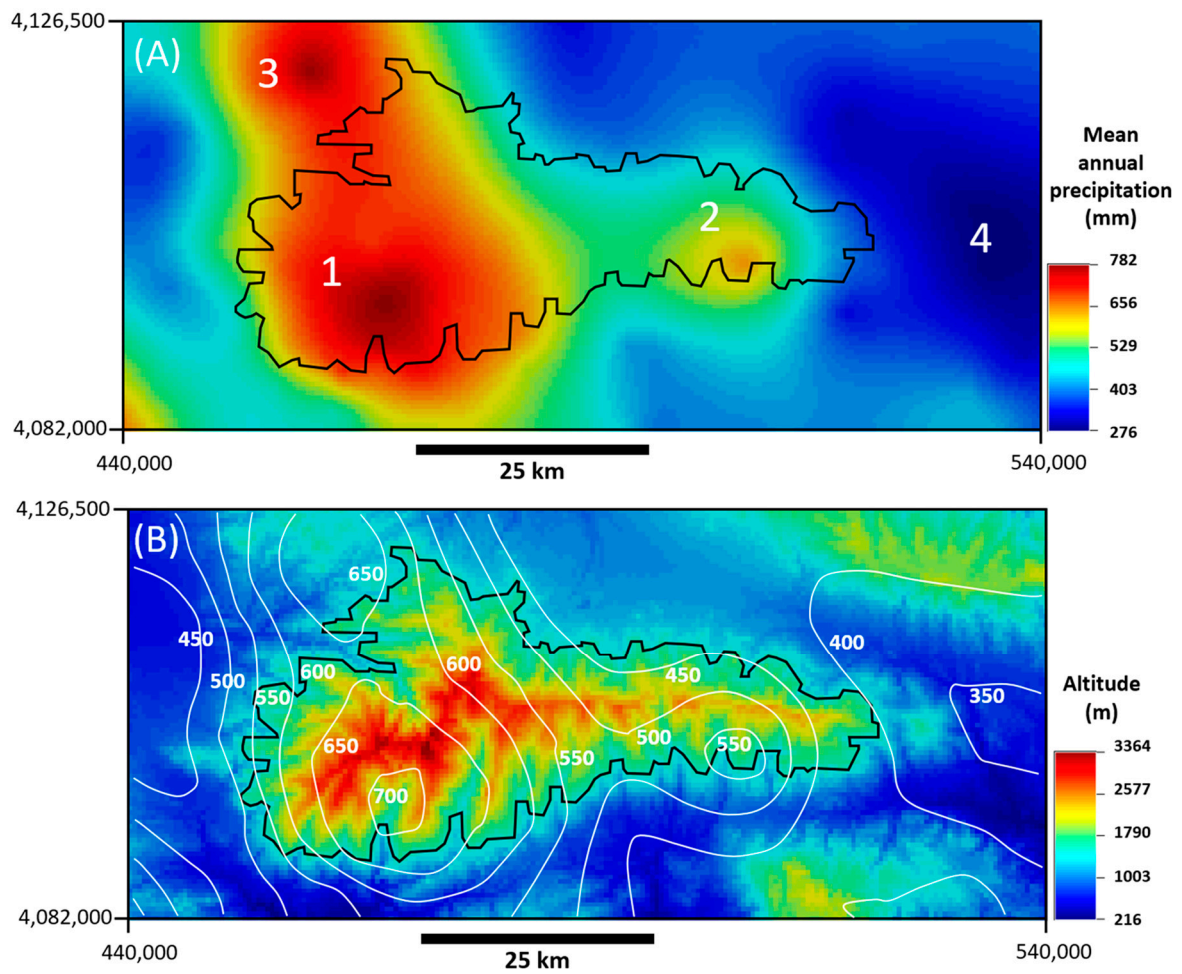


Figure 3. (A). Spatial distribution of the mean annual precipitation for the 1951–2017 period. There are three precipitation maxima: 1 and 2 inside the Sierra Nevada mountain range; 3 is the maximum outside the mountain range and 4 is the region of shadow precipitation on the lee side of the mountain. (B). Same as (A) but as isohyets (solid white lines) overlying the topography map. The black polygon in (A,B) encloses the area of the Sierra Nevada mountain range. Geographical coordinates in the figure are in the Universal Transverse Mercator (UTM) projection.

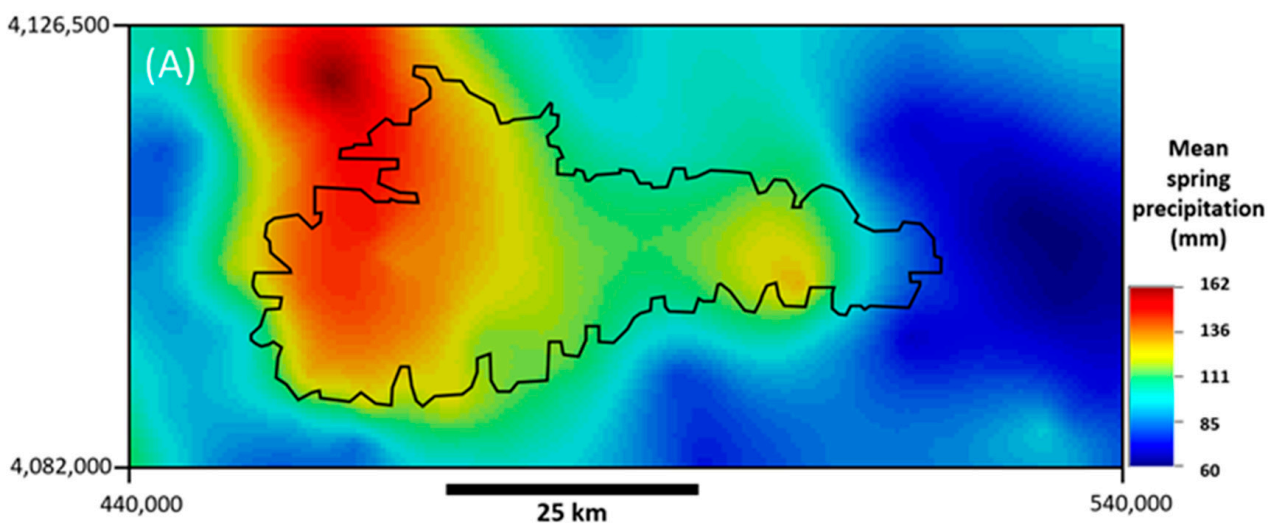


Figure 4. Cont.

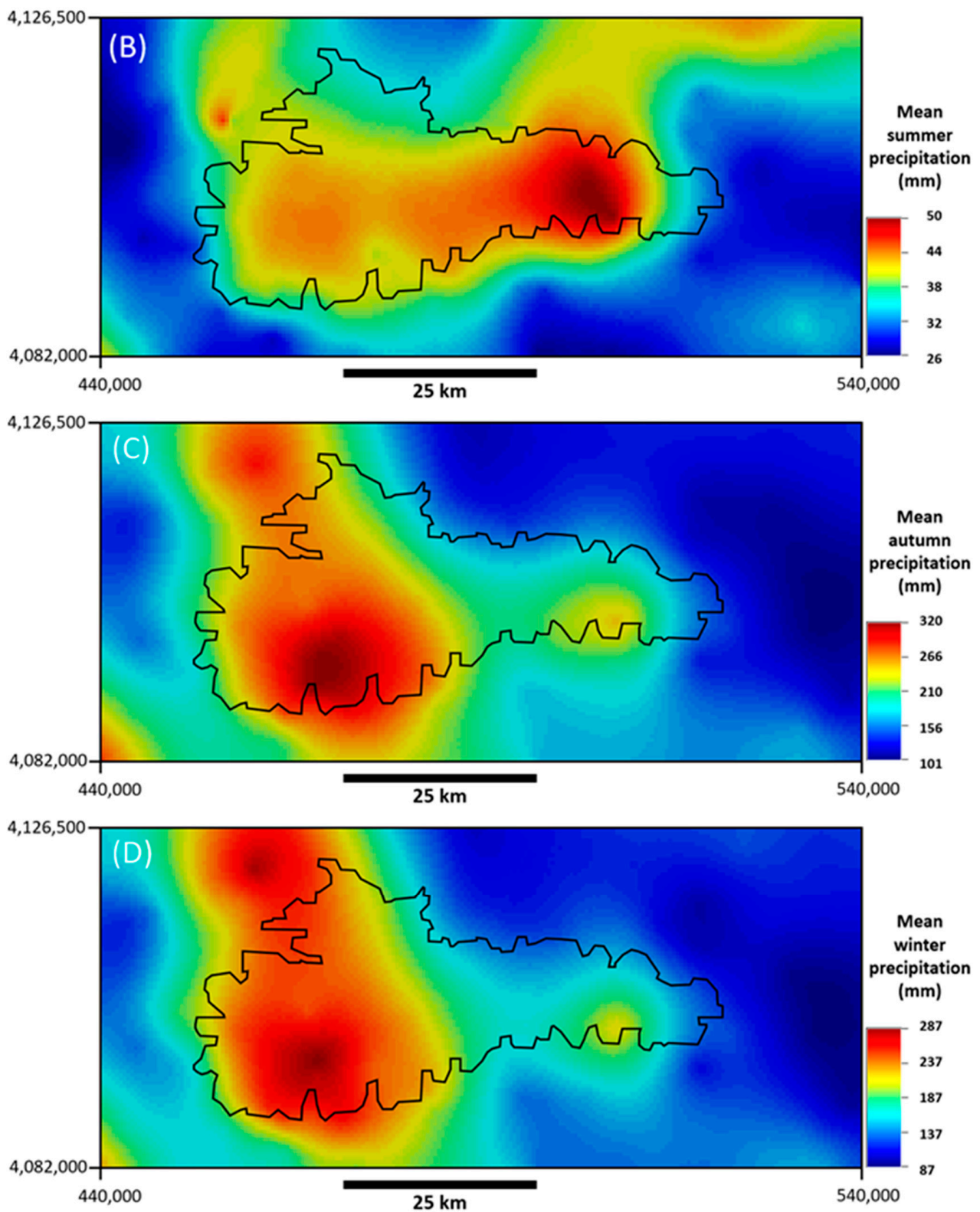


Figure 4. Spatial distribution of the mean seasonal precipitation for the 1951–2017 period. (A). Spring (AMJ), (B). Summer (JAS), (C). Autumn (OND), (D). Winter (JFM). The letters in parentheses are the initials of the consecutive months used to define each season. Geographical coordinates in the figure are in the Universal Transverse Mercator (UTM) projection.

Table 1. The mean annual precipitation in Sierra Nevada for the 1951–2017 period is 575 mm, with a standard deviation of 191 mm. The table shows the way in which this annual precipitation is distributed by months and by seasons.

Month	Mean Precipitation (mm)	% of Annual Precipitation	Season	Mean Precipitation (mm)	% of Annual Precipitation
January	68.0	11.8	Winter (JFM)	197.9	34.4
February	67.5	11.7			
March	62.4	10.8			
April	55.8	9.7	Spring (AMJ)	115.5	20.1
May	41.7	7.2			
June	18.0	3.1			
July	3.9	0.7	Summer (JAS)	39.1	6.8
August	7.0	1.2			
September	28.1	4.9			
October	58.7	10.2	Autumn (OND)	222.9	38.7
November	77.7	13.5			
December	86.5	15.0			

Figure 4 shows that the wettest seasons (Autumn in Figure 4C and Winter in Figure 4D) reproduce the annual mean precipitation shown in Figure 3. The general spatial trend of the annual precipitation in Figure 3 is also reproduced in the other two seasons (Spring and Summer) but with the difference that the maximum precipitation in Spring occurred outside the target area in the north-western sector (number 3 in Figure 3A), while the maximum precipitation in Summer occurred in the second maximum of precipitation inside the target area, located in the eastern part of the Sierra (number 2 in Figure 3A). This behaviour was due to the orographic effect and the provenance of the humid winds, as explained in the discussion section.

Another important result is the mean annual temperature (minimum, maximum, and mean) in the Sierra Nevada for the period from 1951 to 2017, which is represented in Figure 5A–C, respectively. Because of the high negative correlation between temperature and altitude, the temperature maps in Figure 5 clearly resemble the map of altitudes in Figure 1C. The spatial distribution of temperatures can be calculated for any temporal interval as, for example, in Figure 5D, which shows the minimum January temperature for the 1951–2017 period.

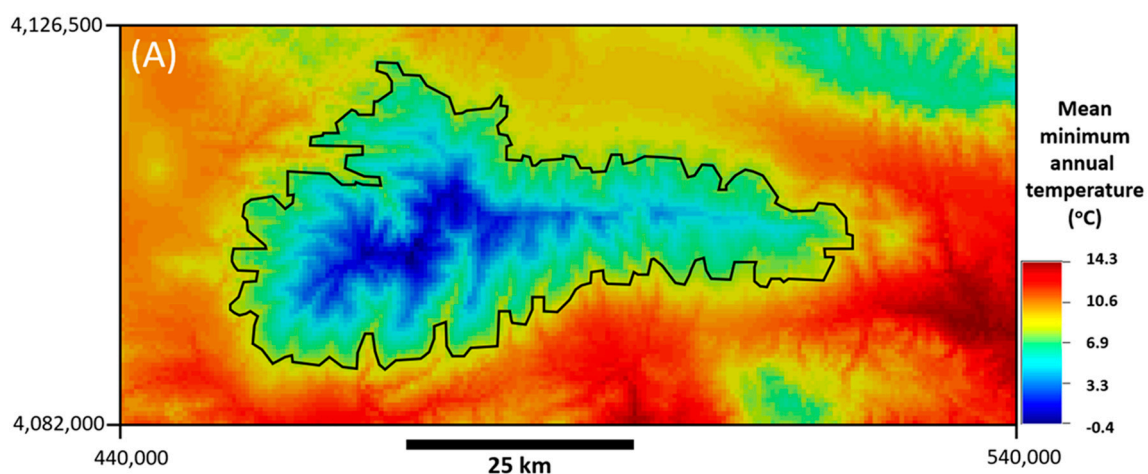


Figure 5. Cont.

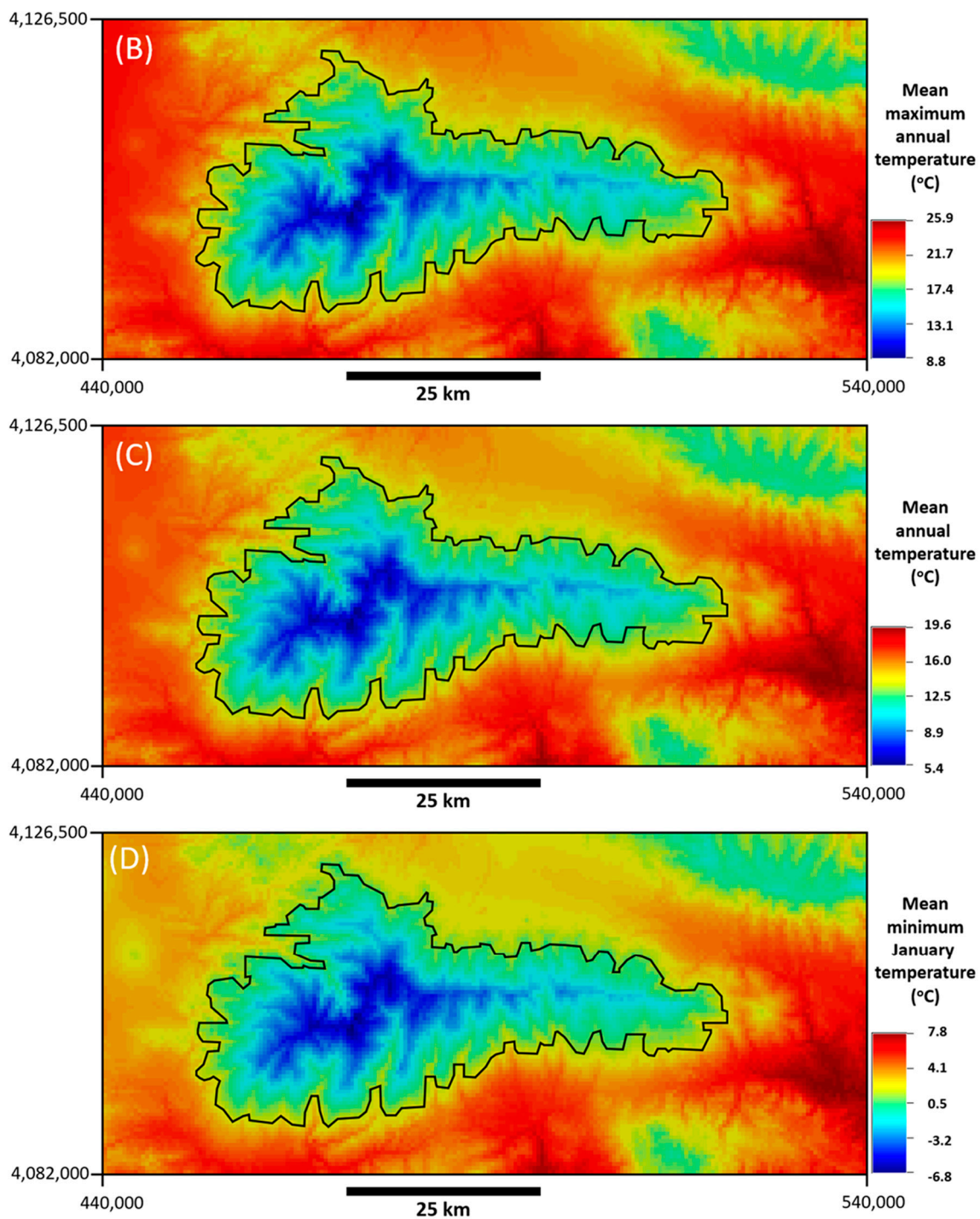


Figure 5. Spatial distribution of the mean temperature for the 1951–2017 period. (A): annual minimum; (B): annual maximum; (C): annual mean; (D): minimum for January. Geographical coordinates in the figure are in the Universal Transverse Mercator (UTM) projection.

Figure 6A shows the spatial variability of the total annual snow obtained by assuming that the daily precipitation when the minimum daily temperature was below zero degrees Celsius would fall in the form of snow. Figure 6B shows that the percentage of total precipitation that fell in the form of snow increased with altitude and, within the Sierra Nevada mountain range, varied from 4.2% to 78.7%, with a mean of 24.9%.

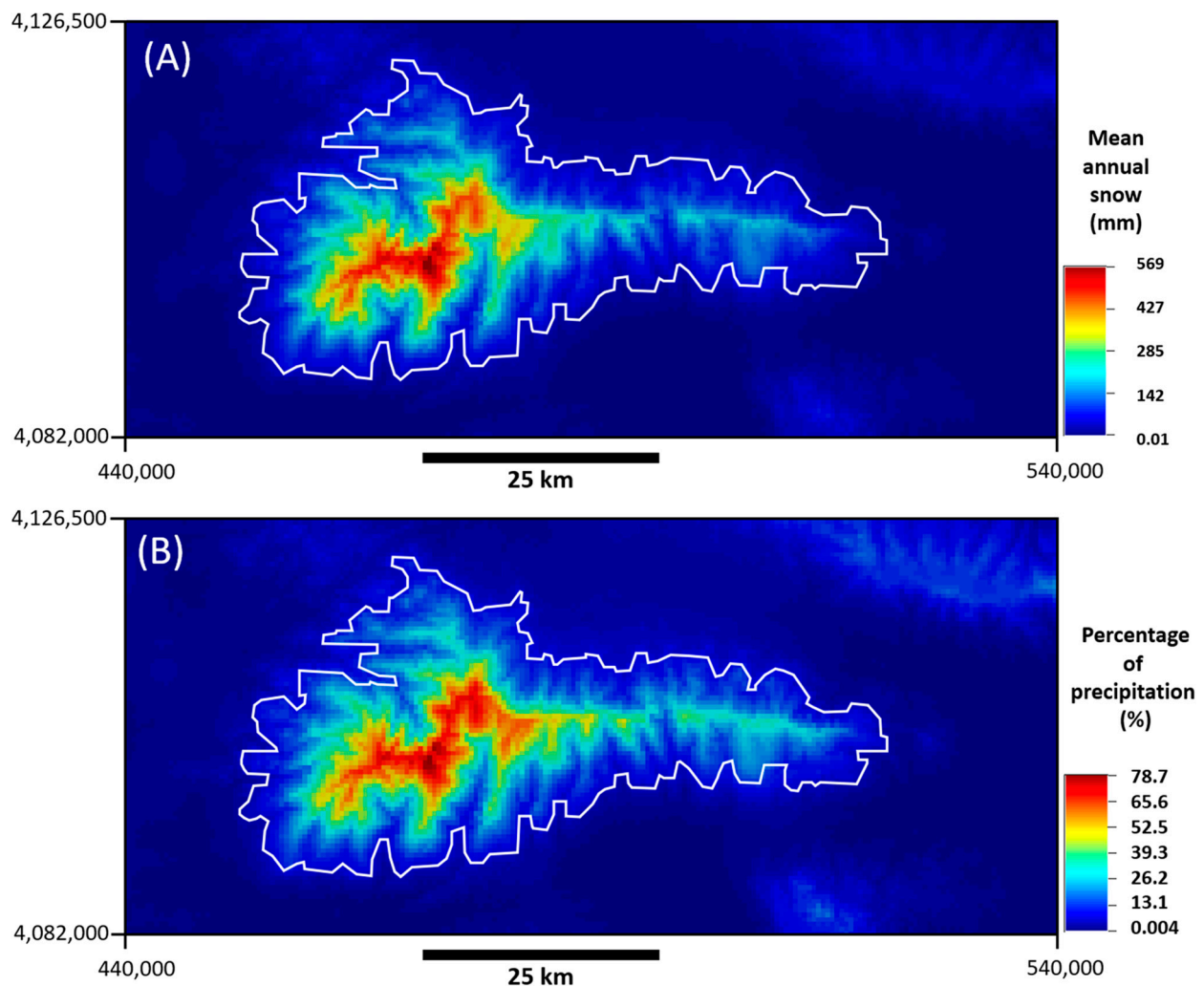


Figure 6. (A). Spatial distribution of the mean annual snow fall for the 1951–2017 period, obtained by considering that daily precipitation was in the form of snow if the daily mean temperature was below 0 °C. (B). Spatial distribution of snow as a percentage of precipitation. Geographical coordinates in the figure are in the Universal Transverse Mercator (UTM) projection.

Another interesting result is the time series of the areal average of the annual precipitation for Sierra Nevada (black polygon in Figure 1C) for the 1951–2017 period, i.e., a period of 67 years or almost seven decades. The estimated time series is shown in Figure 7A. The mean annual precipitation of 575 mm is represented as a horizontal, large-dashed line. The high variability of annual precipitation over the years is reflected in a time series with a standard deviation of 191 mm. Despite this high variability, the annual precipitation decreased linearly at a rate of 33 mm of precipitation per decade. The negative slope is statistically significant (i.e., differs from zero), with a confidence level of 95%. The fitted linear trend is shown as a solid red line in Figure 7A. This decrease can be seasonally decomposed as a decrease of 15 mm in Winter precipitation, 12 mm in Autumn precipitation, and 6 mm in Spring precipitation, while there was no significant change in Summer precipitation. In addition, the years with the lowest precipitation coincided with droughts in southern Spain or in the entire Iberian Peninsula and have been marked with blue arrows in Figure 7A. It is clear from the Figure that the number of droughts increased with time, and it is estimated that a mean precipitation in Sierra Nevada of less than 440 mm is indicative of a drought in the region. A different aspect is the evolution of seasonality, defined here as the percentage of annual precipitation comprising Autumn precipitation. The result is shown in Figure 7B, in which it is clear that seasonality has remained unchanged over the 1951–2017 period.

Seasonality has been defined as the percentage of annual precipitation occurring in Autumn, because Autumn is the main wet season in the area, recording, on average, 40% of the precipitation of the whole year.

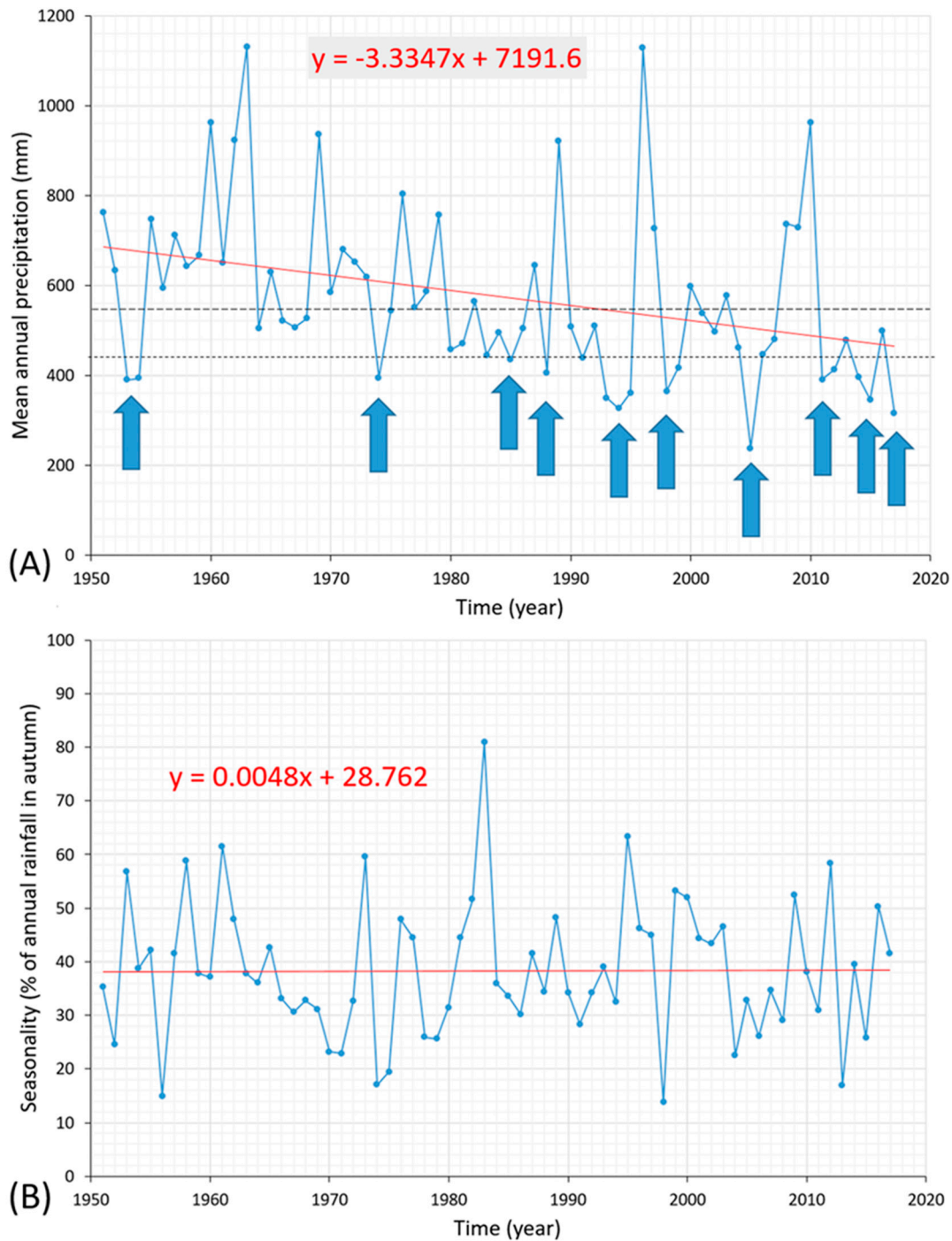


Figure 7. (A) Time series of the mean annual precipitation from 1951 to 2017 in Sierra Nevada. The horizontal long-dashed line represents the global mean of 575 mm. The horizontal short-dashed line represents a threshold value of 440 mm that identifies historical droughts in the region. The solid red line is the trend which shows a decline in mean annual precipitation at a rate of 33 mm per decade. The blue arrows represent the drought years and show that the number of droughts has increased since the mid 1980s. (B) Time series of precipitation seasonality defined as the percentage of annual precipitation occurring in Autumn. Seasonality has remained constant for the 1951–2017 period.

Although Figure 7A shows the time series of the mean total rainfall over the Sierra Nevada mountain range, the same time series can be calculated on a pixel basis to show the spatial variability of the slope of the total rainfall as in Figure 8A. It can be seen that inside the Sierra Nevada limits, the slope is always negative (rainfall decreasing with time), but it is statistically significant (at the 95% confidence level) in the western part and on the northern side of the eastern part.

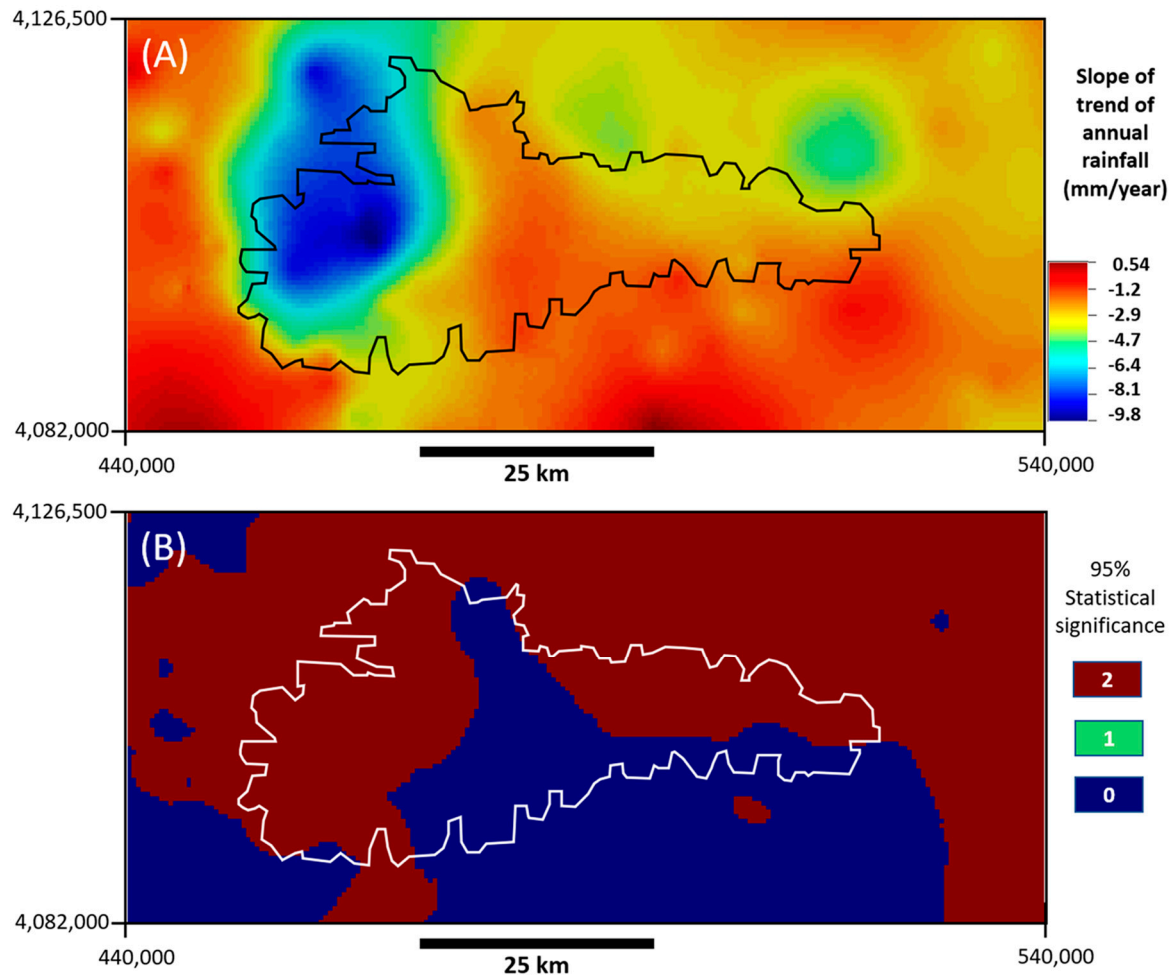


Figure 8. (A) Spatial variability of the slope of the linear trend of mean annual rainfall for the 1951–2017 period. (B) Statistical significance (at the 95% level) of the slope shown in (A). Blue colour (0) implies that the slope is not statistically significant. Green colour (1) implies a statistically significant positive slope, while red colour implies a statistically significant negative slope. The figure shows that there is a decreasing trend in rainfall which may be statistically significant on the western and northern sides of the eastern part of Sierra Nevada. Geographical coordinates in the figure are in the Universal Transverse Mercator (UTM) projection.

A spectral analysis of the time series of mean annual precipitation may reveal hidden periodicities or cycles in precipitation. The maximum entropy method [33,34] was applied to the time series in Figure 7A and the estimated power spectrum is shown in Figure 9. There are important cycles lasting around 12 years, related to sunspot cycles. A cycle of 83 years is also related to solar activity but is less reliable because it is longer than the length of the time series of the available data. The cycles of 6.5, 3.4, and 2.7 years are related to the North Atlantic Oscillation (NAO) index.

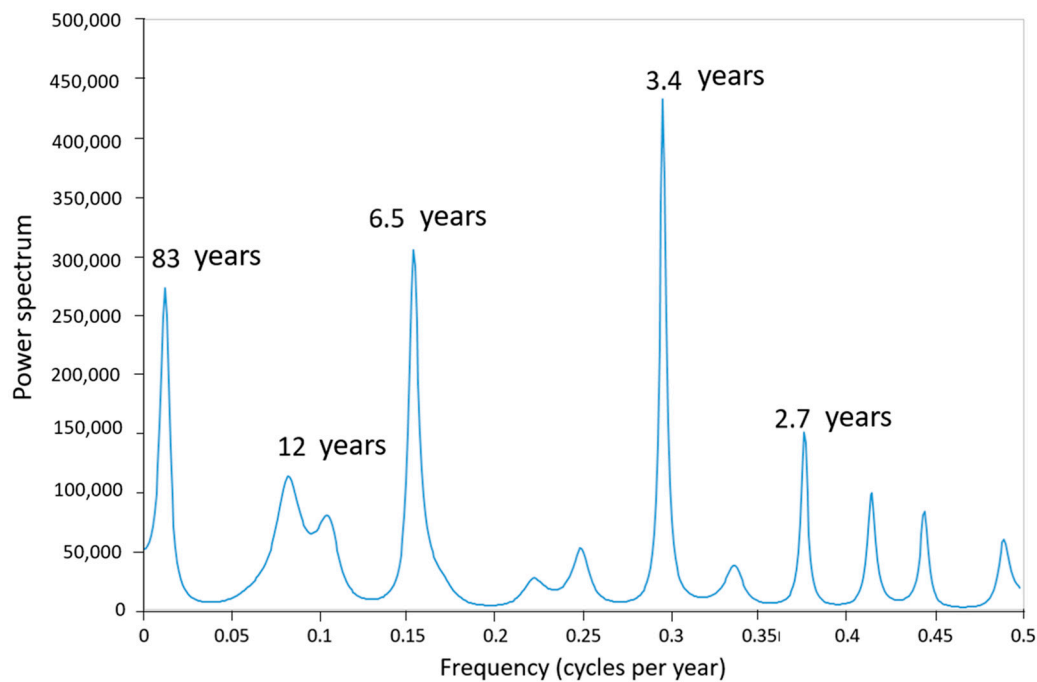


Figure 9. Maximum entropy power spectrum of the time series shown in Figure 5A. There is an important power at 12 years associated with sunspot cycles; 83 years is associated with variability in insolation and with cycles with periods of 6.5, 3.4, and 2.7 years, which have been associated with the NAO index.

The previous suggestion that there may be a relationship between annual precipitation and the annual NAO index has been investigated further. Both variables (annual precipitation and the annual NAO index) are plotted in Figure 10A, in which there is an obvious correspondence of wet years with a negative NAO index, whereas dry years are related to a positive NAO index. This negative relationship can be more clearly seen by comparing the polynomial trends fitted to both time series (thick solid line in Figure 10A). This clear relationship between precipitation in the Sierra Nevada and the NAO index is considered further in the discussion section, as is the issue of the altitudinal precipitation gradient.

With respect to temperature, Figure 11 shows, for the Sierra Nevada mountain range, the time series of minimum, maximum, and mean temperatures for the 1951–2017 period. It is clear from the figure that the slope is negative, which implies that temperature is decreasing at a rate of around 0.1 °C every 10 years, which seems paradoxical in a global warming context. However, it can be shown that all three slopes are statistically significant with a confidence level of 95%. Again, it is instructive to assess the time series of the different temperatures for the different pixels, i.e., the spatial variability of the trend across space, as shown in Figure 12. Figure 12A shows minimum temperature, Figure 12C shows maximum temperature, and Figure 12B,D shows the statistical significance of the different slopes. For both minimum and maximum temperatures, there are positive and negative trends, together with areas that are not statistically significant (at the 95% confidence level), areas that have positive slopes that are statistically significant, and areas that have negative slopes that are statistically significant. For both minimum and maximum temperatures, the statistically significant positive slopes (increasing temperature with time) are in the eastern part of the mountain range, while the statistically significant negative slopes (decreasing temperature) are in the western part of the mountain range.

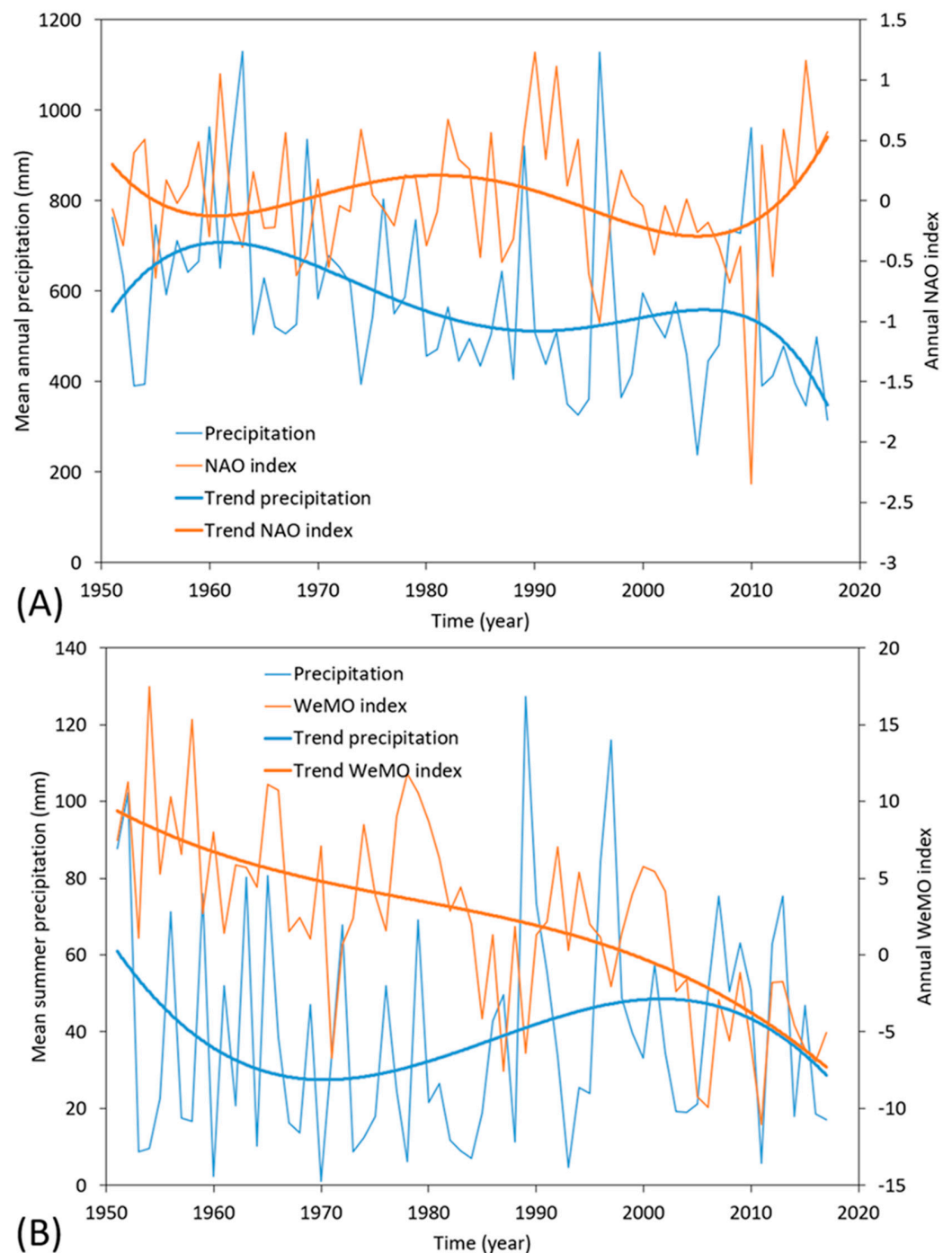


Figure 10. (A) The thin orange solid line is the Hurrell (1995) annual NAO index (based on the difference between the normalised sea level pressure (SLP) at Lisbon, Portugal and Stykkisholmur/Reykjavik, Iceland). The thin solid blue line is the mean annual precipitation (Figure 7A). The polynomial fitted trends are the solid thick lines, orange for the NAO index and blue for the precipitation. The joint variation of the two variables is clear from the figure with high annual precipitation corresponding to high negative NAO indices and vice versa. (B) The thin solid orange line is the Martin-Vide and Lopez-Bustins (2006) annual WeMO index (WeMO is based on the difference between the normalised sea level pressure (SLP) at San Fernando, Spain, and Padua, Italy). The thin solid blue line is the mean Summer precipitation. The polynomial fitted trends are the solid thick lines, orange for the WeMO index and blue for the precipitation. The figure suggests a weak joint variation of the two variables, with high Summer precipitation corresponding to high WeMO indices and vice versa.

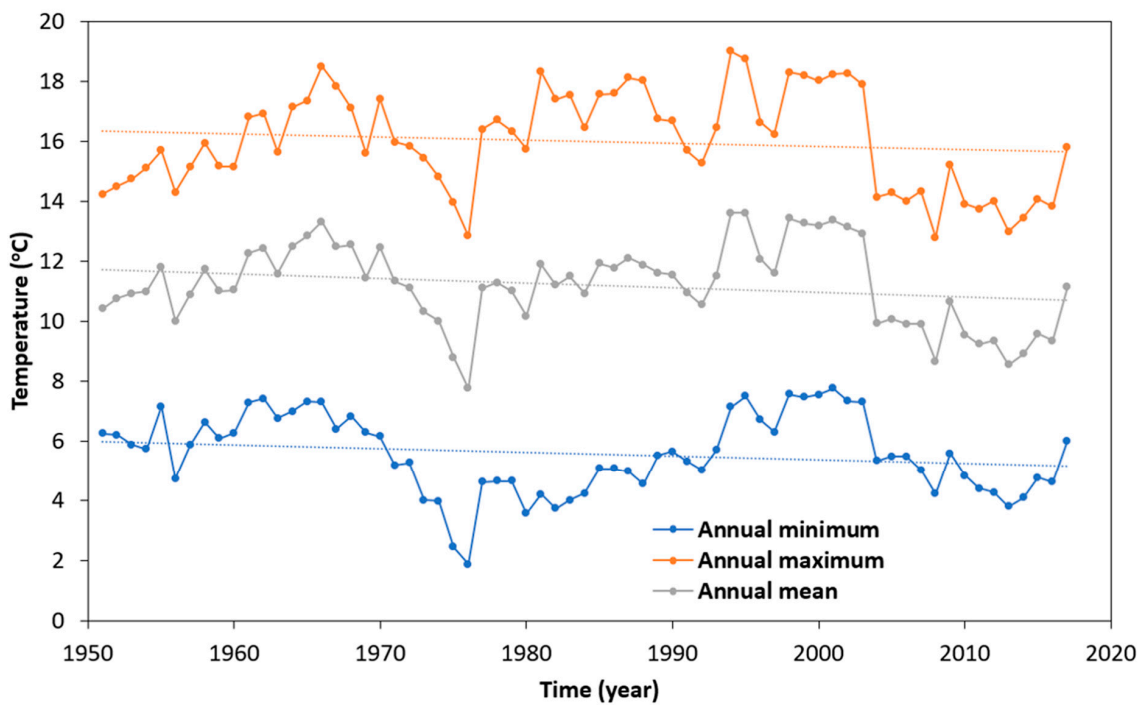


Figure 11. Time series of the minimum, maximum, and mean annual temperatures from 1951 to 2017 in Sierra Nevada. The dashed lines represent the fitted linear trend. In all three cases, the slope is negative and shows a decrease of 0.1 °C every 10 years. However, this negative slope is not statistically significant at the 95% significance level, (i.e., it is not statistically different to zero), and thus, the negative trend in temperature can be neglected when considered over the entire mountain range.

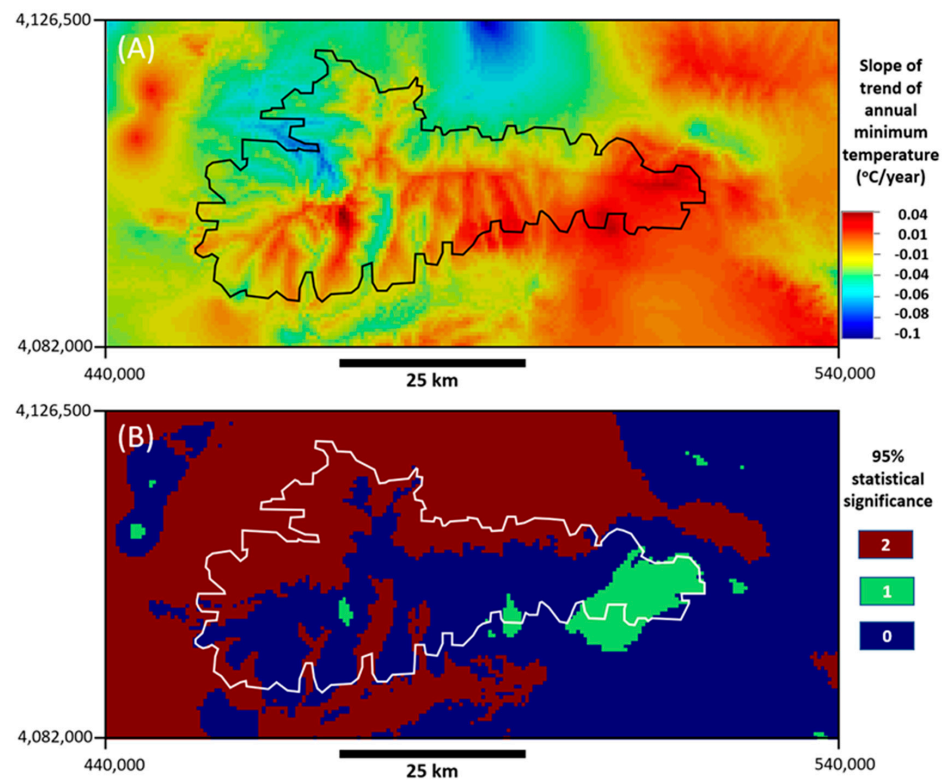


Figure 12. Cont.

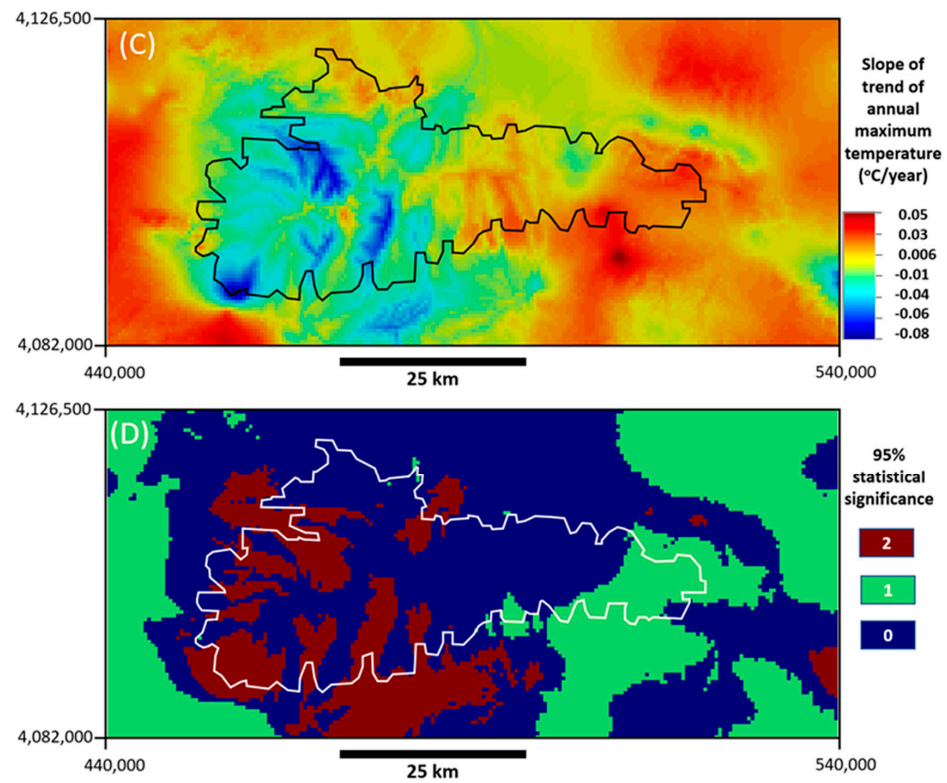


Figure 12. (A) Spatial variability of the slope of the linear trend of the minimum (A) and maximum (C) annual temperatures for the 1951–2017 period. (B,D) show the statistical significance (at the 95% level) of the slopes shown in (A,C), respectively. Blue colour (0) indicates that the slope is not statistically significant. Green colour (1) indicates a statistically significant positive slope, while red colour implies a statistically significant negative slope. The figures show that, for the Sierra Nevada mountain range, the trends in annual minimum and maximum temperatures have a complex behaviour, with increasing and decreasing trends. In the eastern part of the Sierra Nevada mountain range, there is a statistically significant increase in minimum and maximum annual temperatures, while in the western part, there are areas of statistically significant decreases in the minimum and maximum annual temperatures. The geographical coordinates in the figure are in the Universal Transverse Mercator (UTM) projection.

Finally, the equivalent product for snow can be obtained by using a simple snow precipitation and melting model. The adopted model is precipitation in the form of snow when the minimum temperature is below zero degrees Celsius. The melting model used is the temperature index of the snow melt model [35], formulated as:

$$\begin{aligned}
 &\text{If } F_1(i,j,t) \leq F_2 \rightarrow \text{Snow}(i,j,t) = \text{Precipitation}(i,j,t) \\
 &\text{If } F_3(i,j,t) \leq F_4 \rightarrow \text{Snow}(i,j,t) = \text{Snow}(i,j,t-1) - F_5(i,j,t)F_6 \\
 &F_1, F_3, F_5 \in \{T_{min}, T_{max}, T_{med}\} \\
 &F_2, F_4, F_6 \in \mathbb{R}
 \end{aligned}$$

where $\{T_{min}, T_{max}, T_{med}\}$ are the daily minimum, maximum, and mean temperature, respectively.

(i,j,t) : is the cell with spatial location (i,j) for day (t) .

F_2, F_4, F_6 are real numbers. The first two are temperature thresholds and the third is a multiplicative melting factor.

The parameters were selected using a simple calibration that gave the following: $F_1 = T_{min}, F_2 = 0, F_3 = T_{min}, F_4 = 1, F_5 = T_{min}$ and $F_6 = 5$.

Figure 13 shows the experimental snow thickness data given in [36,37]. The thin line represents the point measurements of the changing thickness of snow over a four-

year period at a point located in the Refugio de Poqueira (Sierra Nevada). The thick line represents the pixel measurements of snow from the dataset used in the work presented here and the previous simple model. The changing thickness results are similar but not identical because of the different supports (point and pixel) on which they are measured.

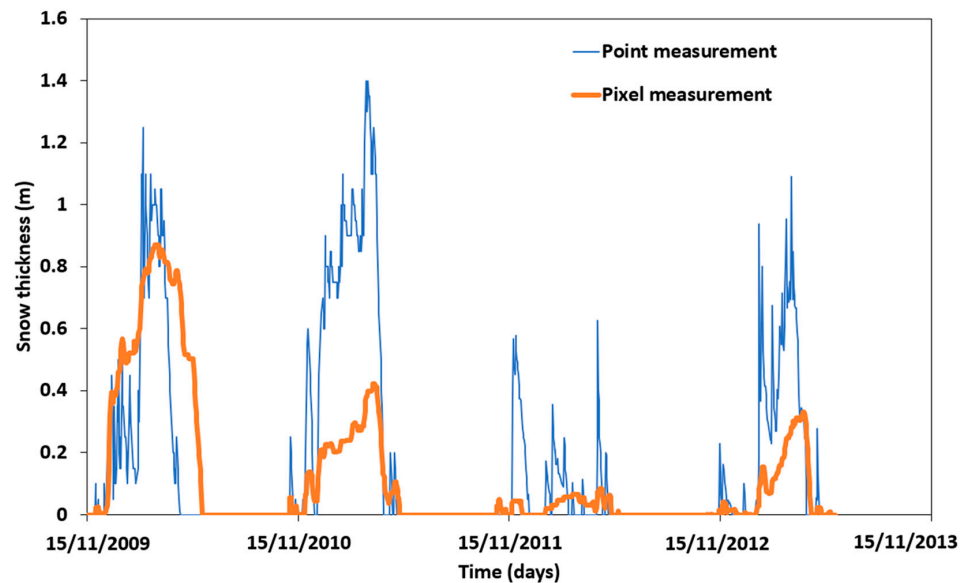


Figure 13. Different aspects of snow dynamics can be obtained by using a simple snow-degree model for melting and assuming that daily precipitation was in the form of snow if the daily minimum temperature was below zero degrees Celsius. Snow depth (m) at a point location from Herrero et al. (2016) [37] compared with the 500×500 m pixel that contains that point from the fields of rainfall and minimum temperature.

Figure 14 shows the changing area of snow cover in the Sierra Nevada mountain range over the 1951–2017 period. Days on which the entire mountain range was covered by snow are recorded as 100% snow cover. The detail of the snow-covered area is given in Figure 15. Figure 16 shows the thickness of snow in the cell that contains the ski resort town of Pradollano.

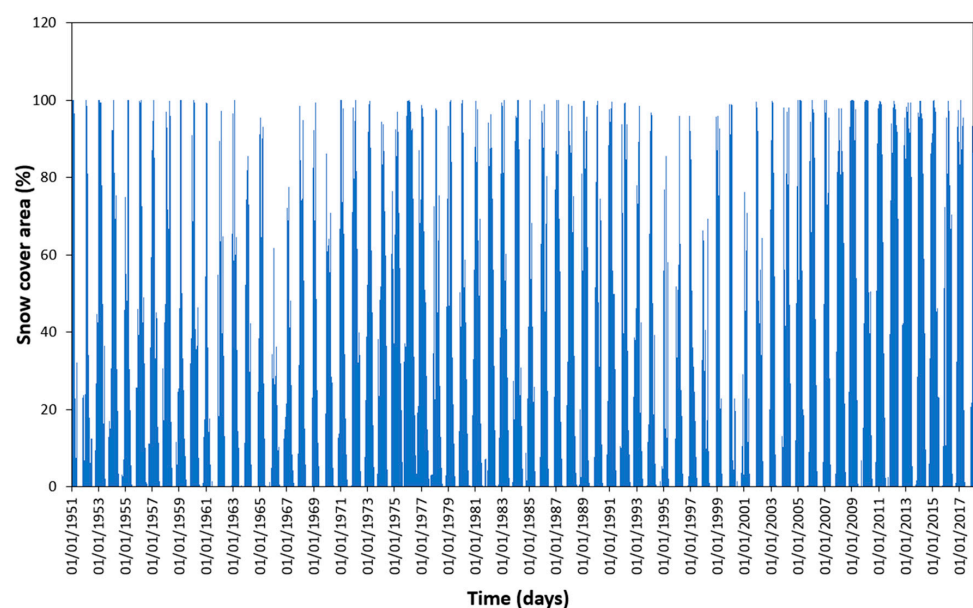


Figure 14. Evolution of the snow-covered area of the snowpack of Sierra Nevada (altitude higher than 1500 m) and shown as the percentage of the Sierra that is covered by snow.

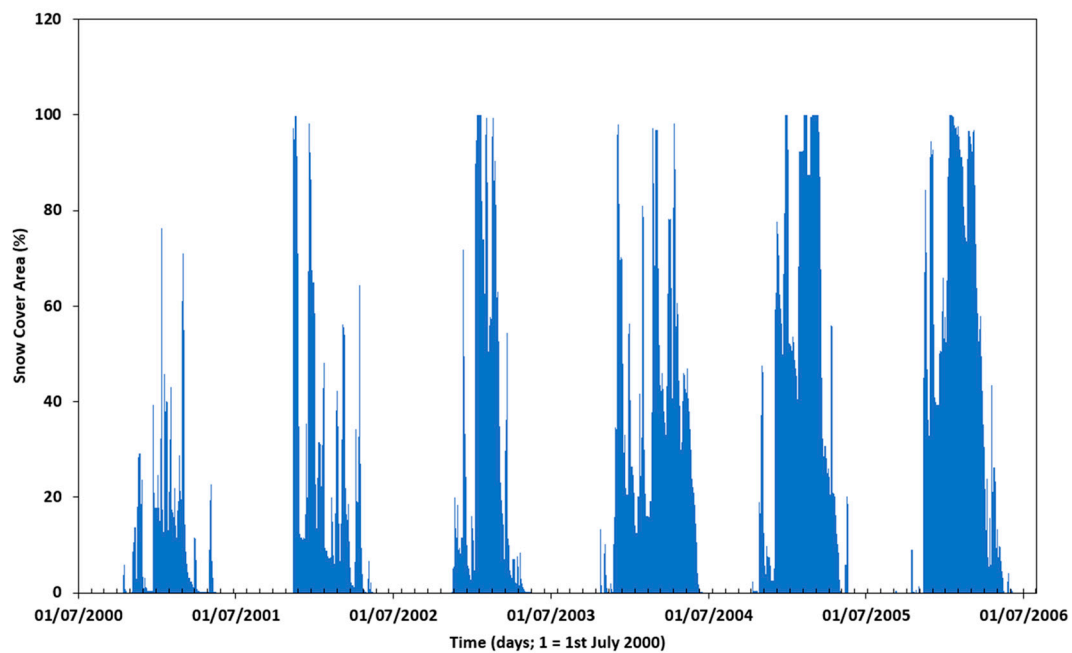


Figure 15. Detail of the snow-covered area for six snow seasons between the years 2000 and 2006.

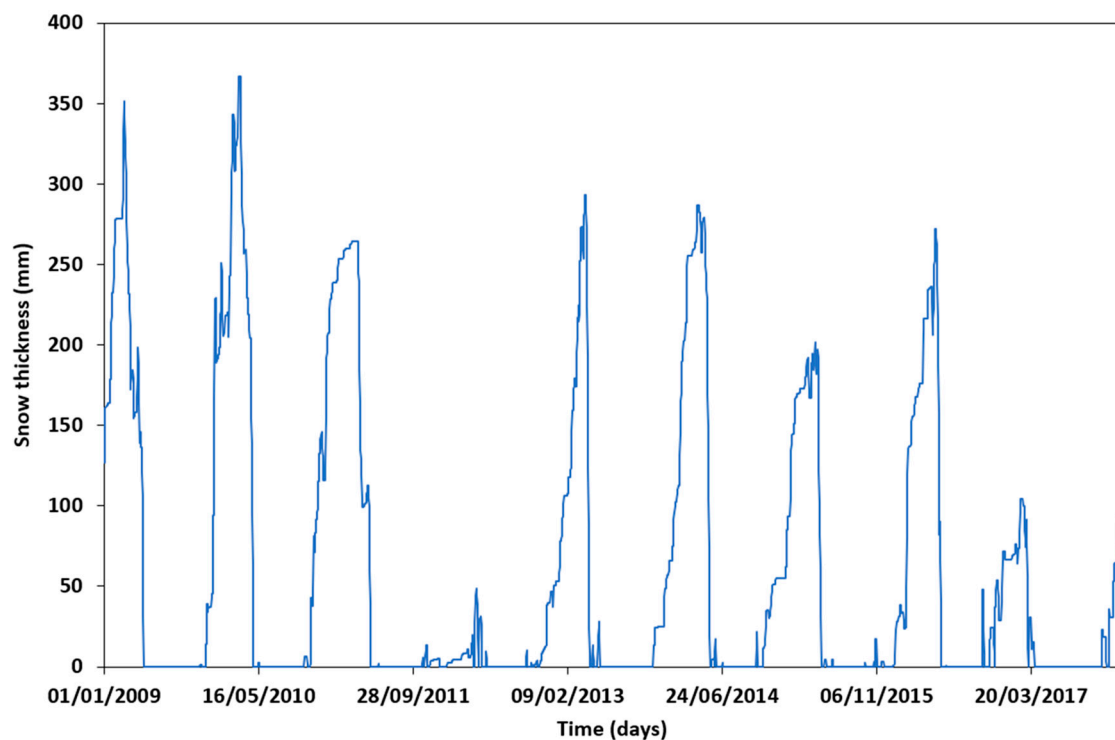


Figure 16. Snow thickness in the pixel that contains the Pradollano ski resort.

5. Discussion

Three important issues in the spatio-temporal dynamics of precipitation in the Sierra Nevada have been identified in this study: (1) the importance of orographic precipitation [38] in understanding the spatial variability of mean annual precipitation; (2) the decreasing trend in the mean annual precipitation of 33 mm per decade; and (3) the NAO influence on mean annual precipitation. Other minor issues that have been revealed are (4) the persistence of seasonality over the almost seven decades studied and (5) the complex issue of the altitudinal precipitation gradient.

The precipitation patterns over the Sierra Nevada mountain range for the period of this study can be interpreted physically by considering the orographic effect and the main provenance of humid flows from the Atlantic and, to a lesser extent from the Mediterranean, that affect the Iberian Peninsula in general and the study area in particular. The authors of [12] distinguished atmospheric patterns with a clear distinction between Atlantic and western Mediterranean disturbances that produce characteristic precipitation patterns over southern Spain. Most of the annual precipitation is drawn from the Atlantic Ocean and is mainly influenced by North Atlantic climatic processes [39], such as the polar cyclone (Iceland Low), and hence the North Atlantic Oscillation (NAO) [40]. Annual precipitation is sourced to a lesser extent from the Mediterranean and is mainly influenced by the Western Mediterranean Oscillation (WeMO) [41]. Isotopic studies [39] revealed two main sources of humidity that influence precipitation in the Mediterranean part of the Iberian Peninsula. Convective precipitation events from the Mediterranean are isotopically enriched and prevail during Summer (Figure 10). In contrast, precipitation with lower isotopic values is transported along Atlantic storm tracks, which dominate during Winter [42]. The authors of [12] distinguished atmospheric patterns (synoptic types) with a clear distinction between Atlantic and western Mediterranean disturbances that produce characteristic precipitation patterns in Mediterranean Spain. In addition, from the synoptic types they obtained, The authors of [12] summarised the main general scenarios that produce significant precipitation in Mediterranean Spain. The first scenario is a large-scale disturbance located to the west of the Iberian Peninsula and producing humid Atlantic flows that induce precipitation in western Andalusia. A second scenario is the passage of cold fronts over the Iberian Peninsula associated with higher latitude, low pressure systems that encourage precipitation in the mountainous areas of Andalusia. In a third scenario, relatively small lows at 500 hPa are found in the southern part of Spain, and the associated low-level flux over the Mediterranean from the east-southeast is warm and humid. This configuration leads to precipitation over the eastern flank of Spain [12]. These three scenarios generated the three maxima in mean annual precipitation shown in Figure 3A.

The observed decreasing trend, at a rate of 33 mm per decade, in mean annual precipitation in Sierra Nevada for the 1951–2017 period is consistent with findings by other authors. A general decreasing trend in precipitation in southern Spain from 1960 onwards was observed by [43]. The authors of [32,44], among others, have also identified this decreasing trend of precipitation in southern Spain. Here, we have shown this decrease in the mean areal value of the high Sierra Nevada mountain range. The authors of [45] studied the evolution over almost 100 years of the Azores high (the “centres of actions” for the weather in the Iberian Peninsula) and concluded that blocking anticyclones have become more prevalent over western Europe, which could explain the decrease in rainfall over the Iberian Peninsula in general and in the Sierra Nevada in particular.

There are clear correlations between the NAO index and the annual precipitation in the Sierra Nevada and between the NAO index and Autumn and Winter precipitation. This is because 73% of the annual precipitation occurs in Autumn and Winter. To a lesser extent, there is a correlation between the precipitation in Sierra Nevada and the WeMO index. The positive phase of the NAO reflects below-normal heights and pressures across the high latitudes of the North Atlantic and above-normal heights and pressures in the central North Atlantic [46]. Hence, there is a northward shift of the axis of maximum moisture transport [47], and thus, there is a decrease in precipitation over southern Europe in general (including Spain) and in the Sierra Nevada in particular.

Despite the variability of the total annual precipitation and its decreasing trend, there was variability, although there was no trend, in the seasonality for the observed 1951–2017 period. Here, seasonality has been defined as the percentage of annual precipitation comprising Winter precipitation. The conclusion is that, irrespective of the trend in annual precipitation, Winter precipitation will be the main seasonal precipitation contribution to the total annual precipitation.

Finally, there is the issue of the complex spatial gradient of mean annual precipitation with altitude. The altitudinal gradient between locations A and B can be defined as:

$$G_{AB} = \frac{R_A - R_B}{H_A - H_B}, \text{ with } H_A > H_B$$

where R_A is the mean annual precipitation at location A and H_A is the altitude of location A. Given that the order of the locations is $H_A > H_B$, a positive gradient means that precipitation increases with altitude. It is clear from Figure 3B that the altitudinal gradient of precipitation for Sierra Nevada will be complex. Because of the orographic effects shown in Figure 3, in the best case (considering the windward side of the Sierra Nevada mountains), there will be an altitudinal gradient in the mean annual precipitation of 15 mm/100 m. There will be a gradient of 10 mm/100 m in the mean annual precipitation for the best location on the lee side of the Sierra Nevada mountains. However, in general, the altitudinal gradients will be smaller if any two arbitrary locations are considered. These altitudinal gradients in precipitation are significantly different to some of the values reported in the literature for the Sierra Nevada mountain range, e.g., 170 mm/100 m reported by [48], among others.

With respect to the spatio-temporal dynamics of temperature in the Sierra Nevada, there are several points that have been identified in this study:

- (1) The spatial distribution of temperature is highly correlated with altitude, with correlation coefficients of 0.85 and 0.9 for minimum and maximum temperature, respectively.
- (2) The annual temperature trend has a negative slope but, as it is not statistically significant, the annual temperature in the Sierra Nevada cannot be considered to be decreasing, even in terms of the minimum, maximum, or mean temperatures.
- (3) The spatial variability of the trend in annual temperatures is complex. There are areas that show an increasing trend while others show a decreasing trend and others are undefined, as the trend is not statistically significant.
- (4) By using a simple degree-day model, it is possible to evaluate the evolution of the Sierra Nevada snowpack by assessing a large number of spatial and temporal statistics. For example, the transient seasonal snowline could be evaluated.

6. Conclusions

A significant database of daily precipitation and temperature on a regular square grid with a spatial resolution of 500 m has been obtained by geostatistical co-kriging, together with an important instrumental record of precipitation and temperatures. The study area for this work is the Sierra Nevada mountain range in southern Spain, restricted to the area with altitude above 1500 m asl, which corresponds to what is generally understood to be the Sierra Nevada mountain range. The main results, based on the precipitation and temperature dynamics of the Sierra Nevada mountains and obtained by a statistical analysis of the high-resolution precipitation database, are the importance of orographic precipitation and the influence of the NAO on the total amount of annual precipitation. The orographic precipitation explains the spatial distribution of the mean annual precipitation with maximum precipitation on the windward side of the mountain. This implies that the highest precipitation is not at the summit of the mountain, as had previously been assumed and which has led to over-estimates of the altitudinal gradient of precipitation for Sierra Nevada. Seasonality has not changed over the 1951–2017 period, for which there are almost seven decades of precipitation records for the most southern alpine environment in Europe. This implies that, irrespective of the total amount of precipitation, most of it will fall in Autumn and Winter. Smith (2019) [49] anticipated that mountain meteorology research would require special attention because of the altered distribution of precipitation, orographic effects, and physical mechanisms by which mountains modify precipitation patterns in different climate zones. Temperature (minimum, maximum, and mean) shows a more predictable spatial behaviour because it is well correlated with altitude. However, the spatial variability of the temperature trend is complex, which makes it difficult to draw

any conclusions about global warming, at least in this area. To address this issue would require a more exhaustive monitoring of mountainous areas and their water resources.

The work reported here is a contribution to the climatological study of alpine environments and should encourage further research in the meteorology and climatology of high mountain areas which store strategic water resources.

Author Contributions: Conceptualization, E.P.-I. and S.M.-R.; methodology, E.P.-I., J.J. and P.A.D.; software, E.P.-I.; validation, E.P.-I. and P.A.D.; investigation, E.P.-I., S.M.-R., J.J. and P.A.D.; data curation, J.J. and S.M.-R.; writing—original draft preparation, E.P.-I. and S.M.-R.; writing—review and editing, J.J. and P.A.D.; supervision, P.A.D.; project administration, E.P.-I. and S.M.-R.; funding acquisition, E.P.-I. All authors have read and agreed to the published version of the manuscript.

Funding: This research was funded by Agencia Española de Investigación (Ministerio de Ciencia, Innovación y Universidades of Spain) grant numbers PID2019-106435GB-I00 and PID2022-140092OB-I00.

Data Availability Statement: The data that support the findings of this study are available on request from the corresponding author.

Acknowledgments: We would like to thank the anonymous reviewers who provided constructive comments that have allowed us to improve the final version of this paper. The compilation of raw meteorological data provided by Mariano Corzo Toscano and Eduardo Martínez Navarrete of the Environment and Water Agency of Andalusia is gratefully acknowledged. We also acknowledge the support of project “Impact, monitoring and assessment of global and climate change on water resources in high-mountain National Parks (CCPM)” (SPIP2021-02741) funded by Organismo Autónomo Parques Nacionales from the Spanish Ministry for Ecological Transition and the Demographic Challenge.

Conflicts of Interest: The authors declare no conflict of interest.

References

- Meybeck, M.; Green, P.; Vörösmart, C. A New Typology for Mountains and Other Relief Classes: An Application to Global Continental Water Resources and Population Distribution. *Mt. Res. Dev.* **2001**, *21*, 34–45. [\[CrossRef\]](#)
- Diaz, H.F.; Grosjean, M.; Graumlich, L. Climate variability and change in high elevation regions: Past, present and future. *Clim. Chang.* **2003**, *59*, 1–4. [\[CrossRef\]](#)
- Beniston, M.; Diaz, H.F.; Bradley, R.S. Climatic change at high elevation sites: An overview. *Clim. Chang.* **1997**, *36*, 233–251. [\[CrossRef\]](#)
- Zamora, R.; Pérez-Luque, J.; Bonet, F.J. Monitoring global change in high mountains. In *Advances in Global Change Research; High Mountain Conservation in a Changing World*; Catalan, J., Ninot, J.M., Mercè Aniz, M., Eds.; Springer: Berlin/Heidelberg, Germany, 2017; Chapter 16; pp. 385–413.
- Palecki, M.A.; Groisman, P.Y. Observing Climate at High Elevations Using United States Climate Reference Network Approaches. *J. Hydrometeorol.* **2011**, *12*, 1137–1143. [\[CrossRef\]](#)
- Toney, J.L.; García-Alix, A.; Jiménez-Moreno, G.; Anderson, R.S.; Moossen, H.; Seki, O. New insights into Holocene hydrology and temperature from lipid biomarkers in western Mediterranean alpine wetlands. *Quat. Sci. Rev.* **2020**, *240*, 106395. [\[CrossRef\]](#)
- Brunsdon, C.; McClatchey, J.; Unwin, D.J. Spatial variations in the average precipitation-altitude relationship in Great Britain: An approach using geographically weighted regression. *Int. J. Climatol.* **2001**, *21*, 455–466. [\[CrossRef\]](#)
- Hu, W.; Yao, J.; He, Q.; Chen, J. Elevation-Dependent Trends in Precipitation Observed over and around the Tibetan Plateau from 1971 to 2017. *Water* **2021**, *13*, 2448. [\[CrossRef\]](#)
- Lancaster, I.N. Relationships between altitude and temperature in Malawi. *South Afr. Geogr. J.* **1980**, *62*, 89–97. [\[CrossRef\]](#)
- Wang, K.; Sun, J.; Cheng, G.; Jiang, H. Effect of altitude and latitude on surface air temperature across the Qinghai-Tibet Plateau. *J. Mt. Sci.* **2011**, *8*, 808–816. [\[CrossRef\]](#)
- Romero, R.; Guijarro, J.A.; Ramis, C.; Alonso, S. A 30 year (1964–1993) daily precipitation data base for the Spanish Mediterranean regions: First exploratory study. *Int. J. Climatol.* **1998**, *18*, 541–560. [\[CrossRef\]](#)
- Romero, R.; Sumner, G.; Ramis, C.; Genovés, A. A classification of the atmospheric circulation patterns producing significant daily precipitation in the Spanish Mediterranean area. *Int. J. Climatol.* **1999**, *19*, 765–785. [\[CrossRef\]](#)
- Rodrigo, F.S.; Trigo, R.M. Trends in daily precipitation in the Iberian Peninsula from 1951 to 2002. *Int. J. Climatol.* **2007**, *27*, 513–529. [\[CrossRef\]](#)
- De Luis, M.; González-Hidalgo, J.C.; Longares, L.A.; Stepánek, P. Seasonal precipitation trends in the Mediterranean Iberian Peninsula in second half of 20th century. *Int. J. Climatol.* **2009**, *29*, 1312–1323. [\[CrossRef\]](#)
- Ruiz Sinoga, J.D.; Garcia Marin, R.; Gabarron Galeote, M.A.; Martínez Murillo, J.F. Analysis of dry periods along a pluviometric gradient in Mediterranean southern Spain. *Int. J. Climatol.* **2012**, *32*, 1558–1571. [\[CrossRef\]](#)

16. Herrera, S.; Gutiérrez, J.M.; Ancell, R.; Pons, M.R.; Frías, M.D.; Fernández, J. Development and analysis of a 50-year high-resolution daily gridded precipitation dataset over Spain (Spain02). *Int. J. Climatol.* **2012**, *32*, 74–85. [[CrossRef](#)]
17. Zhang, X.; Xu, M.; Kang, S.; Wu, H.; Han, H. The spatiotemporal variability in precipitation gradients based on meteorological station observations in mountainous areas in Northwest China. *Theor. Appl. Climatol.* **2024**, *155*, 163–186. [[CrossRef](#)]
18. Stefanidis, S.; Stathis, D. Spatial and temporal rainfall variability over the mountainous Central Pindus (Greece). *Climate* **2018**, *6*, 75. [[CrossRef](#)]
19. Barbero, G.; Moisello, U.; Todeschini, S. Evaluation of the areal reduction factor in an urban area through rainfall records of limited length: A case study. *J. Hydrol. Eng.* **2014**, *19*, 05014016. [[CrossRef](#)]
20. Chang, C.; Chen, Y.; Huang, J.J. Variability of Rainfall Areal Reduction Factors for a Coastal City: A Case Study of Shenzhen, China. *J. Hydrol. Eng.* **2023**, *28*, 05023008. [[CrossRef](#)]
21. Pardo-Igúzquiza, E. Comparison of geostatistical methods for estimating the areal average climatological precipitation mean using data on precipitation and topography. *Int. J. Climatol.* **1998**, *18*, 1031–1047. [[CrossRef](#)]
22. Goovaerts, P. Geostatistical approaches for incorporating elevation into the spatial interpolation of precipitation. *J. Hydrol.* **2000**, *228*, 113–129. [[CrossRef](#)]
23. Ly, S.; Charles, C.; Degré, A. Geostatistical interpolation of daily precipitation at catchment scale: The use of several variogram models in the Ourthe and Ambleve catchments, Belgium. *Hydrol. Earth Syst. Sci.* **2011**, *15*, 2259–2274. [[CrossRef](#)]
24. Myers, D.E. Matrix formulation of co-kriging. *Math. Geol.* **1982**, *14*, 249–257. [[CrossRef](#)]
25. Wackernagel, H. *Multivariate Geostatistics*; Springer-Verlag: Heidelberg, Germany, 2003; 387p.
26. Chilès, J.-P.; Delfiner, P. *Geostatistics: Modeling Spatial Uncertainty*, 2nd ed.; Wiley: New York, NY, USA, 2012; 726p.
27. Lebel, T.; Bastin, G.; Obled, C.; Creutin, J.D. On the accuracy of areal precipitation estimation: A case study. *Water Resour. Res.* **1987**, *23*, 2123–2134. [[CrossRef](#)]
28. Pardo-Igúzquiza, E. Optimal selection of number and location of precipitation gauges for areal precipitation estimation using geostatistics and simulated annealing. *J. Hydrol.* **1998**, *210*, 206–220. [[CrossRef](#)]
29. Goovaerts, P. *Geostatistics for Natural Resources Evaluation*; Oxford University Press: New York, NY, USA, 1997.
30. Isaaks, E.H.; Srivastava, R.M. *Applied Geostatistics*; Oxford University Press: New York, NY, USA, 1989.
31. Journel, A.; Huijbregts, C. *Mining Geostatistics*; Academic Press: New York, NY, USA, 1978; 600p.
32. Sumner, G.N.; Romero, R.; Homar, V.; Ramis, C.; Alonso, S.; Zorita, E. An estimate of the effects of climate change on the precipitation of Mediterranean Spain by the late 21st century. *Clim. Dyn.* **2003**, *20*, 789–805. [[CrossRef](#)]
33. Pardo-Igúzquiza, E.; Rodríguez-Tovar, F.J. MAXENPER: A program for maximum entropy spectral estimation with assessment of statistical significance by the permutation test. *Comput. Geosci.* **2005**, *31*, 555–567. [[CrossRef](#)]
34. Pardo-Igúzquiza, E.; Rodríguez-Tovar, F.J. Maximum entropy spectral analysis of climatic time series revisited: Assessing the statistical significance of estimated spectral peaks. *J. Geophys. Res. Atmos.* **2006**, *111*, D10202. [[CrossRef](#)]
35. Hock, R. Temperature index melt modelling in mountain areas. *J. Hydrol.* **2003**, *282*, 104–115. [[CrossRef](#)]
36. Herrero, J.; Polo, M.J.; Pimentel, R.; Pérez-Palazón, M.J. Snow depth at Refugio Poqueira (Sierra Nevada, Spain) at 2510 m, 2008–2015. *PANGAEA* **2016**. [[CrossRef](#)]
37. Herrero, J.; Polo, M.J. Evapsublimation from the snow in the Mediterranean mountains of Sierra Nevada (Spain). *Cryosphere* **2016**, *10*, 2981–2998. [[CrossRef](#)]
38. Roe, G.H. Orographic precipitation. *Annu. Rev. Earth Planet. Sci.* **2005**, *33*, 645–671. [[CrossRef](#)]
39. Araguas-Araguas, J.; Diaz Teijeiro, M.F. Isotope composition of precipitation and water vapour in the Iberian Peninsula. In *Isotopic Composition of Precipitation in the Mediterranean Basin in Relation to Air Circulation Patterns and Climate. Final Report of a Coordinated Research Project 2000–2004*; IAEA-TECDOC-1453; IAEA: Vienna, Austria, 2005; pp. 173–190.
40. Lionello, P.; Malanotte-Rizzoli, P.; Boscolo, R.; Alpert, P.; Artale, V.; Li, L.; Luterbacher, J.; May, W.; Trigo, R.; Tsimplis, M.; et al. The Mediterranean Climate: An Overview of the Main Characteristics and Issues. *Dev. Earth Environ. Sci.* **2006**, *4*, 1–26.
41. Martin-Vide, J.; Lopez-Bustins, J.-A. The western Mediterranean oscillation and precipitation in the Iberian peninsula. *Int. J. Climatol.* **2006**, *26*, 1455–1475. [[CrossRef](#)]
42. Celle-Jeanton, H.; Travi, Y.; Blavoux, B. Isotopic typology of the precipitation in the Western Mediterranean Region at three different time scales. *Geophys. Res. Lett.* **2001**, *28*, 1215–1218. [[CrossRef](#)]
43. Rodrigo, F.S.; Esteban-Parra, M.J.; Pozo-Vázquez, D.; Castro-Díez, Y. A 500-year precipitation record in Southern Spain. *Int. J. Climatol.* **1999**, *19*, 1233–1253. [[CrossRef](#)]
44. Ruiz Sinoga, J.D.; Garcia Marin, R.; Martinez Murillo, J.F.; Gabarron Galeote, M.A. Precipitation dynamics in southern Spain: Trends and cycles. *Int. J. Climatol.* **2011**, *31*, 2281–2289. [[CrossRef](#)]
45. Davis, R.E.; Hayden, B.P.; Gay, D.A.; Phillips, W.L.; Jones, G.C. The North Atlantic Subtropical Anticyclone. *J. Clim.* **1997**, *10*, 728–744. [[CrossRef](#)]
46. Muñoz-Díaz, D.; Rodrigo, F.S. Impacts of the North Atlantic oscillation on the probability of dry and wet winters in Spain. *Clim. Res.* **2004**, *27*, 33–43. [[CrossRef](#)]
47. Hurrell, J.W. Decadal trends in the North Atlantic Oscillation, regional temperatures and precipitation. *Nature* **1995**, *269*, 676–679. [[CrossRef](#)] [[PubMed](#)]

48. Castillo Martín, A. Parque Nacional de Sierra Nevada. Clima e Hidrología. In *Parque Nacional de Sierra Nevada*; Canseco Editores: Granada, Spain, 2000; pp. 1–7.
49. Smith, R.B. 100 Years of Progress on Mountain Meteorology Research. In *A Century of Progress in Atmospheric and Related Sciences: Celebrating the American Meteorological Society*; American Meteorological Society: Boston, MA, USA, 2019; Chapter 20; pp. 20.1–20.73.

Disclaimer/Publisher's Note: The statements, opinions and data contained in all publications are solely those of the individual author(s) and contributor(s) and not of MDPI and/or the editor(s). MDPI and/or the editor(s) disclaim responsibility for any injury to people or property resulting from any ideas, methods, instructions or products referred to in the content.